Live and let die: lysis time variability and resource limitation shape lytic bacteriophage fitness

Aaron Smith[1], Michael Hunter[2], Somenath Bakshi[3], and Diana Fusco[1*]

[1]Cavendish Laboratory, University of Cambridge
[2]University of British Columbia
[3]Department of Engineering, University of Cambridge
[*]E-mail: df390@cam.ac.uk

Abstract

Bacteriophages (phages) play a critical role in controlling bacterial populations, both in nature and as potential therapeutic agents. Their ability to replicate, compete against each other, and eradicate target cell populations is usually understood through a number of 'life history parameters', traditionally measured by population-level assays, which implicitly average the parameter's value across a large number of infection events. Recent experiments suggest that bacteriophage life history parameters are subject to considerable heterogeneity, raising the question of whether experimental and modelling efforts that do not account for this variability may overlook important factors in phage's behaviour, competitive fitness or therapeutic viability.

Here, using agent-based simulations, we investigate the importance of stochasticity in lysis time and burst size of lytic bacteriophages in two common laboratory competition experiments: serial passage of well-mixed populations and plaque expansion across a bacterial lawn. We find that a phage's analytic growth rate in isolation can be a poor predictor of its fitness advantage in simulated competition experiments. Specifically, when lysis times are tightly distributed, we identify a novel effect we name "population resonance", through which a bacteriophage can display a significant fitness advantage over a competitor with a much greater growth rate in isolation. Our simulations also show that both serial passage and plaque expansion reward variability in lysis time more than expected, by increasing the phage resilience when resources are scarce.

Author Summary

Bacteriophages (viruses that infect bacteria) can be described by a set of attributes called 'life history parameters'. Historically, these parameters could only be measured on-average over large populations. Recent experimental advancements, however, have enabled their quantification at the single-cell-single-virus level, and have revealed that these traits are subject to inherent variability, even for genetically identical viruses infecting genetically identical cells. Here, we explore whether the degree of variability in one particular life history parameter, the lysis time (the time taken for a bacteriophage to infect and kill its host bacteria) might be subject to natural selection, by quantifying its effects on phage's fitness in two simulated competition experiments: serial passage and plaque expansion. Surprisingly, we find that lysis time variability is advantageous in competition even when it reduces the phage's growth rate in isolation. This finding opens the door to future computational and experimental work, as it demonstrates that mean values alone are not sufficient to describe or predict a bacteriophage efficacy, and that models that ignore this variability can overlook viable evolutionary strategies.

1 Introduction

Bacteriophages (phages) play a critical role in controlling bacterial populations both in nature, in which it is estimated that bacteriophages are responsible for 20 to 40% of all cell lysis events globally [1], and in medicine, where they provide a potential solution to the increasing spread of antimicrobial-resistance among human pathogens [2, 3]. In fact, bacteriophages have been successfully used as antimicrobials since Felix d'Herell's experiments on rabbits in 1917 [4, 5], and recent trials have shown encouraging results [6, 7].

Bacteriophages can be described by a number of 'life history parameters', including adsorption rate (how readily the phage binds to target cells), lysis time (the time between adsorption to the cell and lysis), and burst size (the number of offspring released at cell death). The phenotypic assays typically used to measure these parameters were first developed several decades ago, and rely on population-level measurements, which inevitably average a parameter's value across a large number of infection events [8–10]. These assays have very recently seen some innovation to accommodate cell-to-cell variability [11–13], but in experiments focussed on phage evolution, competition and optimality, measuring the population average life history parameters remains the popular approach [14–19].

In parallel to this trend, most computational and theoretical work on bacteriophages has traditionally employed ordinary or partial differential equation methods, modelling the progression from infection to lysis either as an explicit and deterministic delay, [20–23], as an exponential process [24, 25], or as a chain of intermediate steps connected by exponential processes [26]. These approaches assume that the distribution of lysis times will conform to a delta function, an exponential distribution, or an Erlang distribution, respectively. Some such work considers plasticity in viral parameters in response to the availability of nutrients to the bacterial host [27, 28]. Accounting for such extrinsic variation allows for a deeper understanding of phage population and evolutionary dynamics, but the intrinsic variation that exists even between clonal cells in identical conditions [29] (and therefore between infection outcome) remains unexplored.

Agent-based models (ABMs), in which bacteria and/or phages are treated as discrete objects with stochastic behaviour, are particularly well suited to investigate the role of noise in population dynamics. Specifically for phage populations, they have been successfully used to study the evolutionary consequences of a phage permitting or preventing superinfection [30], the physical volume occupied by bacteria in a growing biofilm [31, 32], the decay in heterozygosity at the front of an expanding plaque [33], and the possibility of a phage evolving towards symbiosis [34]. By construction, ABMs introduce a degree of variability, since the progression from each time step to the next is probabilistic, but few [30], to our knowledge, have incorporated explicit heterogeneity in lysis time or burst size.

In stark contrast to the general trend in the field summarized above, very recent experiments suggest that bacteriophages are subject to considerable heterogeneity in adsorption rate [16], lysis time [16, 35, 36] and burst size [12, 16, 37], the latter varying by more than an order of magnitude even in genetically identical cells in homogeneous conditions [37]. Since phages are totally dependent on the molecular machinery of their host, this variability likely arises from the considerable heterogeneity of the target bacteria's internal metabolic state, via the availability of ribosomes [38–40], surface receptors [41, 42] and other critical molecules. Adsorption rate has also been shown to be influenced by environmental conditions such as pH and temperature directly [43]. Experimental and modelling efforts that do not account for such variability may, therefore, overlook critical factors that influence phage's behaviour, competitive fitness or therapeutic viability [44].

In bacterial populations, variability in doubling time has been shown to result in a population growing faster than its mean doubling time would predict [45, 46], but whether this result holds in phage populations is not obvious. A key distinction is that, while a bacterium always produces two offspring per division, bacteriophage burst sizes are much larger, can themselves be stochastic and, crucially, may strongly depend on lysis time. Here, we elucidate the importance of stochasticity in lysis time and burst size in lytic bacteriophage replication by using agent-based simulations that explicitly model lysis time and burst size distributions and their potential inter-dependencies in two common laboratory competition experiments: serial passage of well-mixed populations and plaque expansion across a bacterial lawn. We model the extent of these distributions as under the genetic control of the bacteriophage, and therefore subject to natural selection. As discussed above, the ultimate source of such variation likely comes from the host cells, so we may think of a "noisy phage" as a phage that possesses some genetic mechanism to amplify the biological noise of its host, and vice versa, a "non-noisy phage" as one suppressing it.

We find that a phage's analytic growth rate in isolation is a poor predictor of the outcome of competition experiments in two scenarios. First, both the serial passage and plaque expansion protocols reward variability in lysis time more than expected: a "noisier" phage is able to outcompete a faster growing, less noisy phage. Second, when lysis times are tightly distributed, we observe an effect we name "population resonance", in which one phage displays a significant fitness advantage over a competitor with a much greater growth rate in isolation. Both of these phenomena arise from the resource-limited nature of the phage environment and reveal distinct strategies that a phage can adopt to outlive its viral competitors.

2 Methods

2.1 Lytic bacteriophages can be described by seven life history parameters

The lytic cycle (Fig. 1a) begins with a phage particle (virion) adsorbing to the surface of a susceptible cell. The virion then injects its genetic material (DNA or RNA, depending on the phage species), which hijacks the cell's molecular machinery. The cell is forced to synthesise many copies of the phage's proteins and genome, before finally producing lysis proteins, which cause the cell to lyse (burst), releasing the assembled virions [47, 48]. Virions then seek new prey through passive diffusion, and may stochastically denature.

To compare and predict the action of different bacteriophage strains, we employ a widely-used model [23, 25, 27, 28, 33, 49] in which a bacteriophage is described by seven life history parameters (table 1 and Fig. 1a).

α	Adsorption rate [ml min^{-1}]: rate at which free virions bind to susceptible cells. The chance for a virion to find a bacterium and adsorb to it in time dt is $\alpha B dt$ for bacterial concentration B.
β	Burst size [-]: number of new virions produced in each lysis event.
τ	Lysis time [min], also called 'latent period': time between a virion first adsorbing to a healthy cell and cell lysis.
δ	Decay rate [min^{-1}]: rate at which free virions become unviable.
D	Diffusion rate [μm^{2}s^{-1}]: rate at which free virions diffuse through the medium.
ε	Eclipse period [min]: time between a virion first adsorbing to a healthy cell, and the first viable new virion being assembled.
m	Maturation rate [min^{-1}]: rate at which virions are assembled inside the cell, following the eclipse period.

Table 1: Viral life history parameters, their units and definitions.

Importantly, these life history parameters do not vary independently, as physics and biology impose both interdependencies and absolute limits. For instance, to release more virions at lysis (greater burst size, β), a cell must undertake virion production for longer (greater lysis time, τ) or assemble virions faster (greater maturation rate, m). We model this dependency through equation 1. This equation has previously been used to describe the assembly of T7 virions by prematurely and externally lysing host cells [19], as well as to relate the lysis times and burst sizes of a number of mutants derived from the same ancestral strain of bacteriophage λ [23]. That is, it allows one to predict $\beta(t)$ for $t \leq \tau$ for a given bacteriophage genotype, and to predict $\beta(\tau)$ for a number of related mutants.

$$\beta = \begin{cases} 0 & \tau < \varepsilon \\ m(\tau - \varepsilon) & \tau \geq \varepsilon \end{cases} \tag{1}$$

According to this model, the number of viable virions within a cell increases linearly with time, after some initial eclipse period (Fig. 1b). It is assumed [23] that τ may be under selection pressure and adapt when a bacteriophage is introduced to a new environment, but that m and ε remain fixed by absolute biological constraints (for a given combination of phage genotype, bacterial genotype and environmental conditions). That is, m and ε cannot be further optimised by mutation of the bacteriophage alone. This assumption is necessary as, using this model, a larger value of m and smaller value of ε are always better. The possibility of cell-to-cell variation in m is discussed in section 2.2.

Equation 1 introduces a strategic decision between producing fewer offspring quickly and more offspring slowly. The consequences of these strategies on a bacteriophage's population-level growth rate, as well as how variability in lysis time implies variability in burst size are discussed in the following section.

2.2 Variation in lysis time implies correlated variation in burst size

Assuming virions are produced according to equation 1, there are several possibilities as to how stochasticity in lysis time (τ) may create correlated variation in burst size (β).

(i) If lysis time stochasticity arises purely from variation in the duration of the eclipse period and no variability in production time is observed, no correlated variation in burst size is expected (Fig. 1c). Burst size may still vary from cell-to-cell owing to intrinsic stochasticity in maturation rate, but, crucially, burst size and lysis time will be uncorrelated at the single-cell-single-virion level. We label this possibility the 'normal' model.

(ii) If lysis time stochasticity arises purely from variation in the post-eclipse period of active virion production, then given the lysis time of an individual virion, we can predict the burst size of that virion by applying equation 1 directly (Fig. 1d). We label this the 'linear with eclipse' model, or just 'eclipse' model.

(iii) If lysis time stochasticity affects both the eclipse and post-eclipse proportionately, the relative variation in burst size will be equivalent to the relative variation in lysis time (e.g., 20% reduction in lysis time will lead to 20% reduction in burst size, Fig. 1e). We label this the 'Linear' model.

In the following, we consider each of these three models as a biological possibility, and determine in which cases variability in lysis time is advantageous. We focus on variability in lysis time specifically, as variability in burst size alone has little to no effect on a bacteriophage's ability to propagate itself or clear a cell culture (Fig. S1).

2.3 Bacteriophage growth rate can be predicted by numerical integration

We consider a bacteriophage with lysis time distribution $p(\tau)$, and burst size $\beta(\tau)$, and predict its growth rate under the assumption that bacteria are abundant, and therefore: (a) adsorption is instantaneous, and (b) the probability of adsorbing to an already-infected cell is vanishingly small.

Under these assumptions, the population of bacteriophages as a function of time (V_t) is

$$V_t = V_0 e^{kt}, \tag{2}$$

where the effective growth rate k is given by

$$k = \int_0^\infty \frac{p(\tau)\ln\beta(\tau)}{\tau} d\tau, \tag{3}$$

which can be computed numerically for any distribution $p(\tau)$.

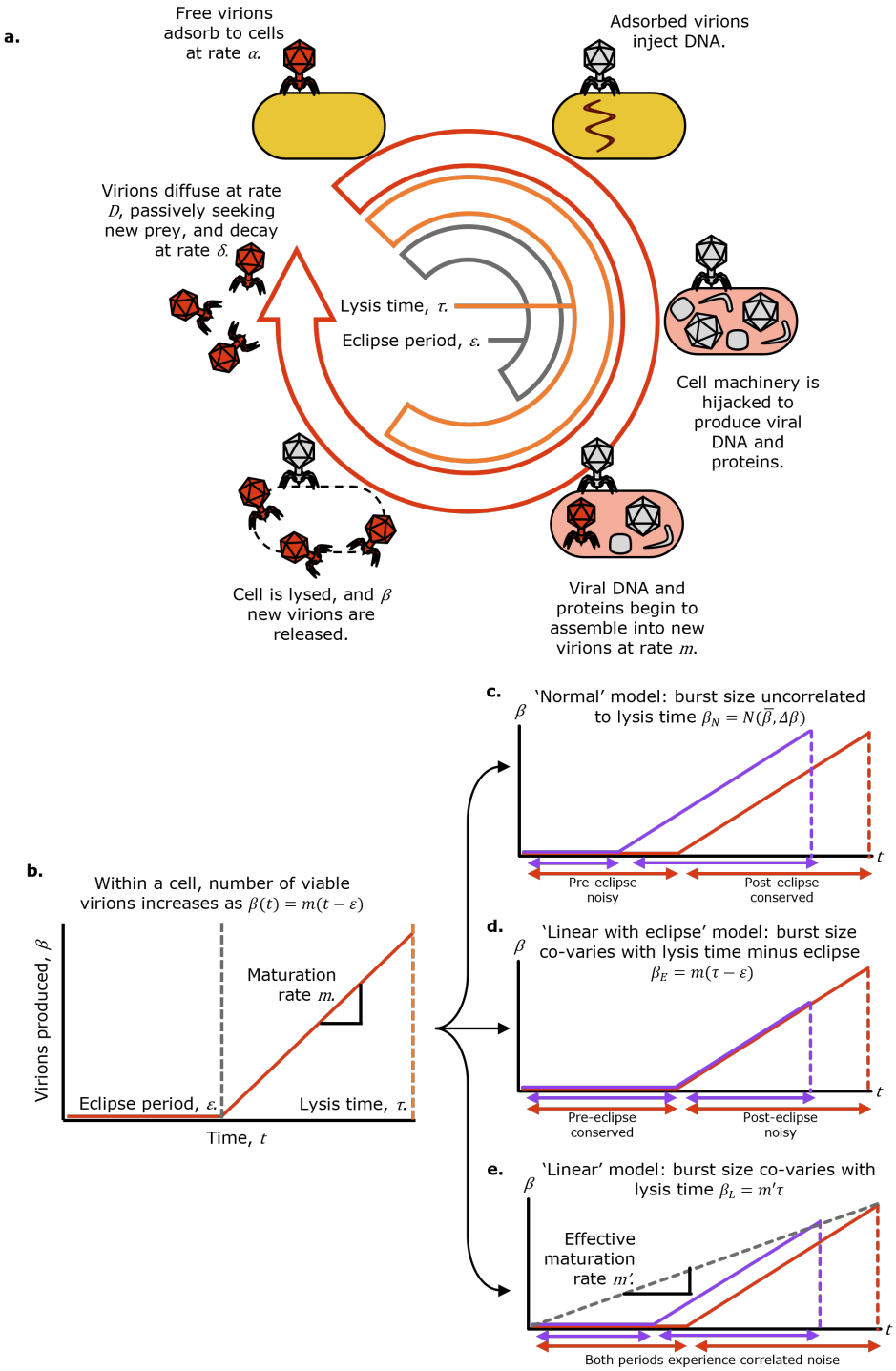

Figure 1: **a.** Schematic of bacteriophage lytic cycle, characterised by seven life history parameters. **b.** Assembly curve, showing the number of viable virions within an infected cell as a function of time: initially zero until the eclipse period elapses, then increasing linearly. **c** to **e.** Assembly curves, each showing the effect of a faster-than-average lysis cycle (purple) versus the average (red), assuming the cycle is faster because the eclipse period is shorter (**c**), the post-eclipse is shorter (**d**), or both are proportionally shorter (**e**).

2.4 Agent-based simulation of two-phage competition experiments

The numerical calculation of the effective growth rate k derived above provides a measure of phage selective advantage under the assumption that resources (bacteria) are so abundant that phages do not meaningfully compete against each other. In real case scenarios, including laboratory experiments, phages always interact, if nothing else because of competition for resources. To assess the competitive fitness advantage of a phage population under different stochastic models, we implement two types of agent-based simulations, mimicking two distinct common laboratory protocols used in the study of bacteriophage evolution: serial passage (spatially unstructured)[14, 50] and plaque expansion (spatially structured)[51, 52]. The former is characterized by a total well-mixed volume Vol of 10^{-5} ml (carrying capacity 100,000 cells) initialized with 10,000 uninfected cells at random points in their cell cycle. The latter is modelled as a one-dimensional series of spatial 'demes', each corresponding to a length Δx of 10µm, and volume Vol of 10^{-7} ml (carrying capacity 100 cells), initialized with 100 uninfected cells at random points in their cell cycle.

Each bacterial agent is characterized by two internal clocks, one representing its own cycle of growth and division and the other representing a count down to lysis, as well as an infection state: 'healthy', 'infected (wild type)' or 'infected (mutant)', and an initially empty list of adsorbed virions. Phage populations are modelled as counters V_i that monitor how many free phages of a specific type are present at any point in time and space. In each simulation time-step, Δt, 'bacterial growth', 'adsorption', 'infection', 'lysis', 'decay' and 'diffusion' substeps occur (Fig. 2).

Adsorption (Fig. 2 step 1): the number of adsorption events for each phage strain is drawn from a Poisson distribution with mean $\alpha(B+I)V_i\Delta t/Vol$, where B is the local number of uninfected bacteria, I is the total local number of infected bacteria, and Vol is the local volume. A bacterial target, sampled randomly and with replacement, is then associated to each of these events. Adsorptions have a chance to fail proportional to the number of phages already adsorbed to the target cell, representing the finite number of receptor sites each cell possesses. The phage population counter is then updated depending on the number of successful adsorption events.

Infection (Fig. 2 step 2): Uninfected bacteria that have at least one adsorbed phage move to an 'infected (wild type)' state or 'infected (mutant)' state according to the nature of the adsorbed phages. In the case where a cell has adsorbed phages of both types, the type of infected state is chosen binomially using the proportion of adsorbed phages of each type. Once a cell becomes infected, the lysis time is drawn from a normal distribution $\mathcal{N}(\overline{\tau}, \Delta\tau)$ where $\overline{\tau}$ and $\Delta\tau$ correspond to the lysis time mean and std of the infecting phage, the lysis-clock starts, and the growth-clock is paused. We note that in this setup, there is no benefit to a bacteriophage that adsorbs to an already-infected cell at a later time step, since the first successful infection immediately and permanently determines the cell's fate.

Growth (Fig. 2 step 3): Uninfected bacteria advance their growth-clocks. If the growth clock completes its cycle, the cell is duplicated. A new growth cycle length is drawn for both mother and daughter cells from a normal distribution.

Lysis (Fig. 2 step 4): infected cells advance their lysis-clocks. If the lysis clock completes its cycle, the cell is deleted, and a number of free phage of the appropriate type are added to their corresponding population counter. Depending on the stochasticity model, this number may be drawn from a distribution, or calculated from the total lysis time.

Decay (Fig. 2 step 5): each phage strain's population counter is reduced by a number drawn from a Poisson distribution with mean $\delta V \Delta t$.

Diffusion (only for plaque expansion, Fig. 2 step 6): the number of migrating phages from one deme to its neighbours is drawn from a Poisson distribution with mean $DV\Delta t/(2\Delta x^2)$ and the corresponding phage population counters are appropriately updated.

Treadmill (only for plaque expansion, Fig. 6a): to allow the infection front to propagate for longer without having to simulate a very large number of demes, we take a 'sliding window' approach. If the deme with the largest number of free virions (total across both pools) is more than 30 demes from the leftmost deme (300µm, or 50% of the total spatial extent X of the simulation), the leftmost deme is deleted, all other demes

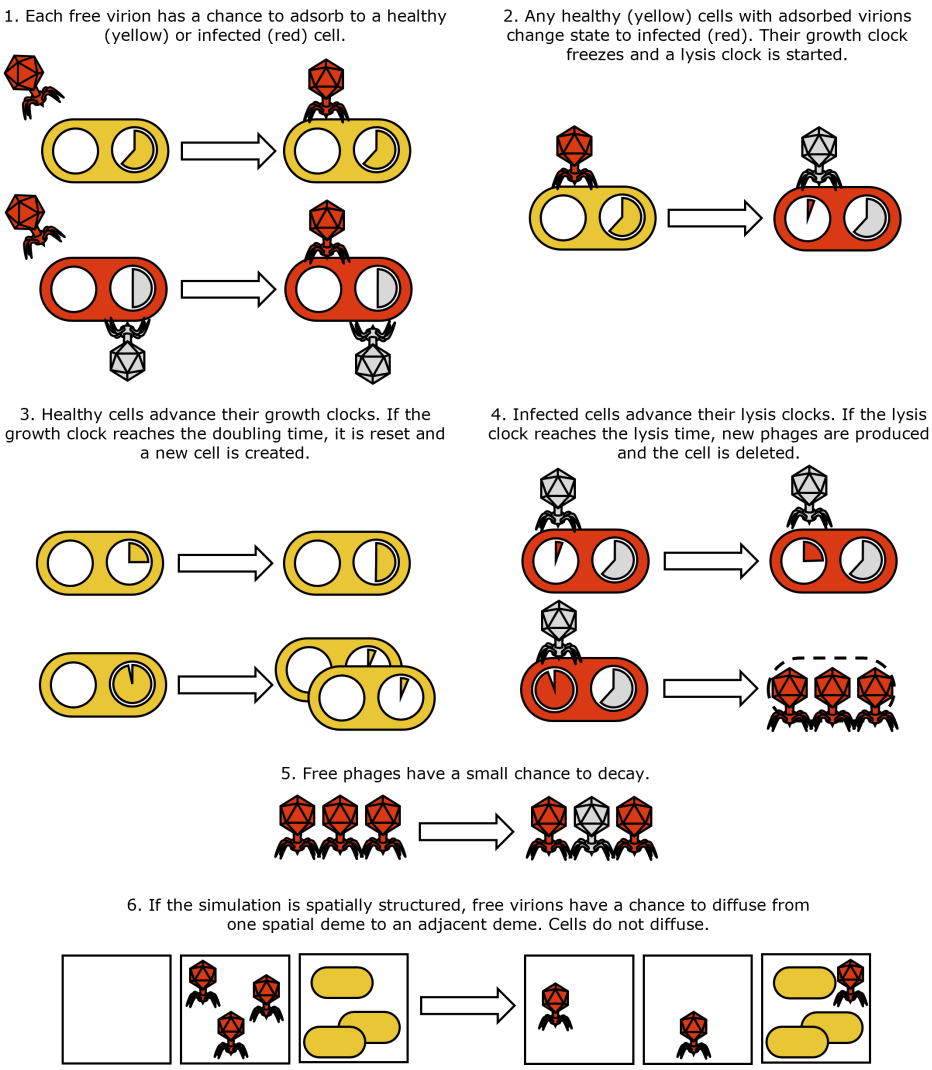

Figure 2: Schematic description of the agent-based model's implementation. Healthy cells and progressing growth clocks are pictured yellow. Infected cells, viable virions and progressing lysis clocks are red. Virions that have injected their DNA, or that have decayed are pictured grey, as well as bacterial growth clocks which have halted due to infection.

are shunted one position to the left, and a new deme is created at the right hand edge of the simulation.

Transfer (only for serial passage, Fig. 4a): if the total number of bacteria falls below 100 (1% of its initial value), we perform a 1000X dilution, so that every remaining bacterium (infected or uninfected) and free phage has 1 in 1000 chance of being transferred to a fresh volume containing 10,000 new uninfected cells.

Both protocols are initialised with 2 pools of 100 phage each, one labelled 'wild type', the other labelled 'mutant'. In the 'plaque expansion' all phages are initially placed in the leftmost deme. The serial passage simulations run either until one phage pool outnumbers the other 70:30, at which point it is declared the winner, or for a maximum of 600 minutes. The plaque expansion simulations always run for 180 minutes. The parameter values used in both these simulations are as follows (tables 2 to 5).

Serial passage parameters		
Vol	10^{-5}	Volume [ml]
T	600	Maximum simulated time [min]
dt	0.01	Timestep [min]
B_0	10,000	Initial bacteria count [cells]
C	100,000	Carrying capacity [cells]
V_0	100	Initial bacteriophage count [virions per strain]

Table 2: Parameters used in serial passage simulations.

Plaque expansion parameters		
Vol	10^{-7}	Volume [ml per deme]
T	180	Total simulated time [min]
dt	0.01	Timestep [min]
X	600	Total simulated length [μm]
dx	10	Deme length [μm]
B_0	100	Initial bacteria count [cells per deme]
C	100	Carrying capacity [cells per deme]
V_0	100	Initial bacteriophage count [virions per strain]

Table 3: Parameters used in plaque expansion simulations.

Bacteria parameters		
$\overline{\tau}_D$	20	Mean doubling time [min]
$\Delta\tau_D$	2	Doubling time std [min]
$A_{\max}$	100 or 1*	Maximum number of adsorbed virions [virions]

Table 4: Bacteria parameters used in all simulations. Values were chosen to agree with published values for *E. coli*, under ideal conditions, but do not represent any particular strain [53]. *$A_{\max}$ was set to 100, aside from those experiments in which super-adsorption was disabled by setting it to 1.

Bacteriophage parameters		
α	3×10^{-9}	Adsorption rate [ml min^{-1}]
$p(\tau)$	$\mathcal{N}(\overline{\tau},\Delta\tau)$	Lysis time probability distribution, taken to be a normal distribution (or delta function in the limit $\Delta\tau\to 0$)
$\overline{\tau}$	17 or varied*	Mean lysis time [min]
$\Delta\tau$	2.5 or varied*	Lysis time std [min]
ε	9.5**	Eclipse period [min], used in 'linear with eclipse' burst size model.
m	20**	Maturation rate [virions min^{-1}], used in 'linear with eclipse' burst size model.
m'	8.82**	Effective maturation rate [virions min^{-1}], used in 'linear' burst size model.
$\overline{\beta}$	150**	Mean burst size [virions], used in 'normal' burst size model.
$\Delta\beta$	50	Mean burst size std [virions], used in 'normal' burst size model.
δ	$0.01^{\dagger}$	Decay rate [min^{-1}]
D	4	Diffusion rate [μm^{2}s^{-1}]

Table 5: Bacteriophage parameters used in numerical analysis and simulations. Values were chosen to agree with a range of published values for bacteriophage T7, but do not represent any particular strain [8, 44, 50, 54]. *This parameter was either varied within a range, or assigned the value given here. **These Values were chosen such that, in all 3 models, a mean lysis time $\overline{\tau}$ of 17 minutes corresponds to a burst size β of 150. $^{\dagger}\delta$ was set to 0.01, aside from those experiments in which decay was disabled by setting it to 0.

3 Results

3.1 Numerical calculations provide theoretical expectations for optimal lysis times

In section 2.3, we describe how a bacteriophage's effective growth rate k may be numerically predicted. In Fig. 3a, we report this prediction as a function of mean lysis time for a standard deviation of either 0 or 2.5 minutes, respectively, for the three burst size models. Parameters were chosen to be similar to those of bacteriophage T7, and can be found in table 5. An analysis of the sensitivity of our results to these choices can be found in Figs S10 and S11. In the following: (i) the eclipse period ε was taken to be 9.5 minutes, (ii) under all three models, a lysis time τ of 17 minutes leads, by construction, to a burst size β of 150, and (iii) the lysis time distribution, $p(\tau)$, used is Gaussian, and therefore symmetric. Asymmetric lysis time distributions are considered in SI Figs S2 to S5.

For the deterministic case (std = 0 min), the effective growth rate k decreases with increasing lysis time under the 'normal' and 'linear' models. By contrast, the 'linear with eclipse' model exhibits an optimum lysis time value due to the trade-off between long lysis times leading to very slow replication and short lysis time being unproductive because of the eclipse period. This preference for intermediate lysis times has been observed experimentally in serial passage experiments [14]. We emphasise that the fact that shorter lysis times lead to proportionately smaller bursts, as in the 'linear' model, is not sufficient to create an optimal lysis time under exponential growth conditions: the smaller burst size is always more than compensated for by the faster lysis cycle. The existence of this optimum depends entirely on a non-zero eclipse period ε.

When variability in lysis time is introduced, both the 'normal' and 'linear' models display an increase in growth rate compared to their deterministic counterparts. Mathematically, this feature can be explained by the convexity of the growth rate function: the mean of a symmetric sample about a given point will yield a greater value than the point itself. Importantly, the variation is symmetric in lysis time. Symmetric variation in lysis rate would cause a decrease in growth rate [55], since the function would no longer be convex. Conversely, the 'linear with eclipse' model, which features a concave function for short lysis times, is characterized by a reduction in growth rate with the optimal value shifting rightward (Fig. 3 b,c). Under this model, the noisier a phage's lysis cycle is, the longer its lysis time should be. This phenomenon holds across a range of values, as shown in Fig. 3 d,e,f.

Many other probability distributions can be used to investigate the role of noise. A biologically intuitive choice for lysis time distribution is the positively-skewed Erlang distribution, as it describes the stochasticity in waiting time from a series of n (shape) consecutive reactions, each occurring with rate λ (rate). An Erlang with shape $n = 1$ is simply an exponential distribution. We find that the behaviour of the effective growth rate is qualitatively similar to that obtained using the Gaussian distribution (SI Fig. S2): "Normal" and "Linear" models favour short mean lysis time and large variance (low shape), while the "Linear with Eclipse" model favours an intermediate optimal mean lysis time and small variance (high shape). A similar trend is also observed for the Weibull distribution (SI Fig. S3). To look specifically at the effect of asymmetry in the distribution, we have also considered a skew normal (SI Fig. S4). Interestingly, we see that, for given mean lysis time, negative skew is beneficial in the 'Normal' and 'linear' models, as it provides additional weight to short lysis times, while positive skew is beneficial in the 'eclipse' model, as its short left tail limits the occurrence of very short unproductive lytic cycles. Given the qualitative similarities between the different distributions, in the following, we focus on the easily interpretable Gaussian distribution.

3.2 Serial passage competition experiments reveal winning strategies beyond growth rate maximisation

In section 2.4, we described a stochastic, agent-based model of the bacteriophage lytic cycle, which allows us to explicitly model the consequences of variability in a bacteriophage's burst size and lysis time. We start by using this model to investigate how the phage fitness landscape is affected by (i) the different types of trade-off between lysis time and burst size encoded in our models (Fig. 1c-e), and (ii) the level of noise in lysis time. We consider two bacteriophage populations, labelled "wild type" and "mutant", and assign them both the same burst size model ('normal', 'linear', or 'linear with eclipse') and the same standard deviation

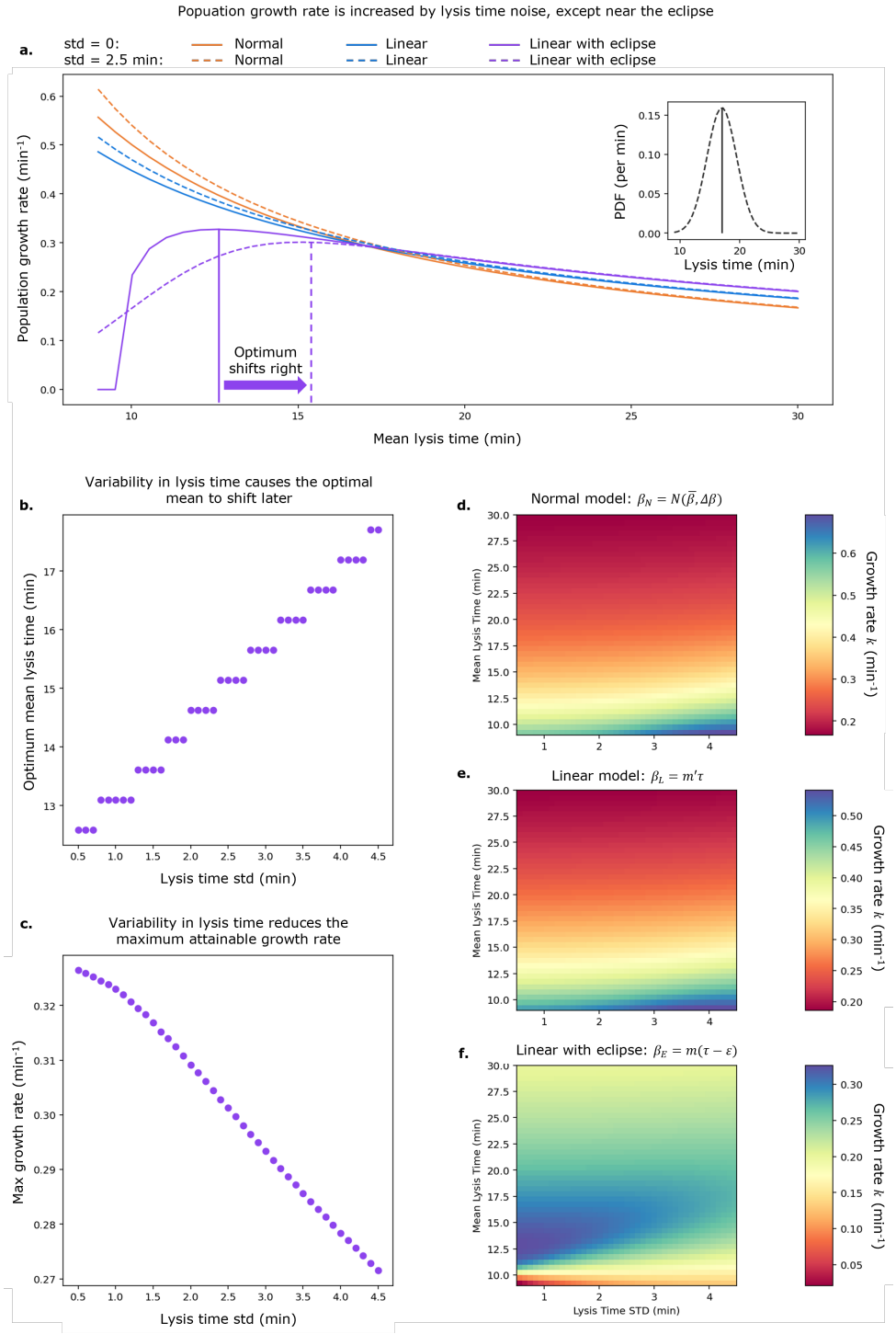

Figure 3: **a.** Bacteriophage effective growth rate k as a function of mean lysis time, with either 0 minutes or 2.5 minutes standard deviation in lysis time. Inset: example lysis time distributions with mean 17 minutes, std 0 (solid line) or 2.5 minutes (dashed line). **b.** Optimal lysis time under 'linear with eclipse' model as a function of lysis time std. **c.** Effective growth rate achieved at optimal lysis time, under 'linear with eclipse' model, as a function of lysis time std. **d.** to **f.** Effective growth rate as a function of both mean lysis time and lysis time std for 'normal', ''linear', and 'linear with eclipse' models respectively.

in lysis time (0.01 or 2.5 minutes). We then vary the mean lysis time of each between 10 and 30 minutes in one-minute increments, and compete the two phage populations against each other through a serial passage assay (Fig.4 a, section 2.4). (Fig. 4b).

For each set of simulation parameters, we quantify competitive fitness using three alternative measures: (i) the numerically predicted difference in effective growth rate k (defined in eq. 3) between the two phages (Fig. 4b i); (ii) the mutant fixation probability defined as the fraction of twenty independent runs in which the mutant fixes in the population (see section 2.4, Fig. 4 b ii); (iii) the rate of fixation of the mutant (positive values) or wild-type (negative values) strain (Fig. 4b iii), defined as

$$\Delta F = \frac{\mathrm{d}}{\mathrm{dt}}[\ln(V_{\mathrm{mu}}/V_{\mathrm{wt}})], \tag{4}$$

which is derived in SI section 7.2.

In every case red corresponds to the wild type displaying a fitness advantage and blue to the mutant displaying a fitness advantage. By construction, the plots are antisymmetric about $y = x$, therefore in the discussion below we will focus on the bottom-right half of the diagram without loss of generality.

Starting with the leftmost column, corresponding to the 'normal' model with narrow lysis time distribution (0.01 minutes standard deviation), the top row (numerically predicted growth rate) replicates the results in Fig. 3 showing that short lysis times lead to a fitness advantage. The middle row (mutant fixation probability) corroborates this numerical result. The bottom row, (mutant fixation rate), reveals an interesting finding. First, we see that while in the majority of parameter space the rate of fixation agrees in sign to the relative growth rate (top row), the rate of fixation increases much more slowly as we move away from the $y = x$ line. This result reflects how the competition for resources (unaccounted for in the relative growth rate) dramatically screens the fitness advantage that a fast lysing phage would be expected to have when grown in isolation (Fig. S8, S12). A similar result was also observed in ref [30] and highlights how phage fitness estimates based on growth in isolation can be misleading and overestimate the fitness (dis)advantage of a population.

The second unexpected result is the appearance of a "stripe" corresponding to intermediate values (green) of fitness advantage within an otherwise highly advantageous region of parameter space (blue). Along this stripe, the mutant lyses cells faster than the wild type and reaches fixation as we would expect. However, it reaches fixation more slowly (in more serial passage cycles) than in the surrounding parameter space.

Close investigation of these cases reveals that they arise due to the limited number of cells available (SI Fig. S7a). The faster-growing mutant experiences a substantial "dead time" after completing its final round of lysis, just before the transfer step takes place. During this period, the only cells remaining are those infected by the (slower-lysing) wild type. The mutant virions, therefore, have no way to further proliferate, and are only subject to decay or unproductive super-adsorption. As a result, by the time the wild type finishes its final round of lysis, there are fewer mutant virions left to survive the dilution.

In line with this explanation, the lower edge of the stripe, highlighted with a white line, corresponds to $y = x/2$: the longest possible dead time (and thus the least advantageous parameters for the mutant phage in this region) would occur when the end of the mutant's final round of lysis happens just after the start of the wild type's final round. When the mutant's lysis time becomes half of that of the wild type, it will be able to begin a new round of lysis at the same time as the wild type's final round, with minimal dead time (SI Fig. S7b).

As additional support to our explanation, we repeat all simulations in Fig. 4b but under "conservative" conditions, in which free virions do not decay and super-adsorption cannot occur (SI Fig. S8). As expected, under these conditions the stripe disappears, as the mutant phage suffers no penalty from spending "dead time" outside the cell. We refer to this phenomenon as "population resonance", since it occurs only for specific ratios $\tau_{\mathrm{mu}}/\tau_{\mathrm{wt}}$ and for specific initial cell counts B_0 (Fig.S12), which determine the number of lytic cycles occurring between dilutions.

The second column ('normal' model, 2.5 mins lysis time std) qualitatively agrees with the first. The only quantitative difference is that the stripe caused by population resonance appears blurred. Since here lysis times for both phages are more variable, lysing events are less synchronised, and the resonance effect is weaker.

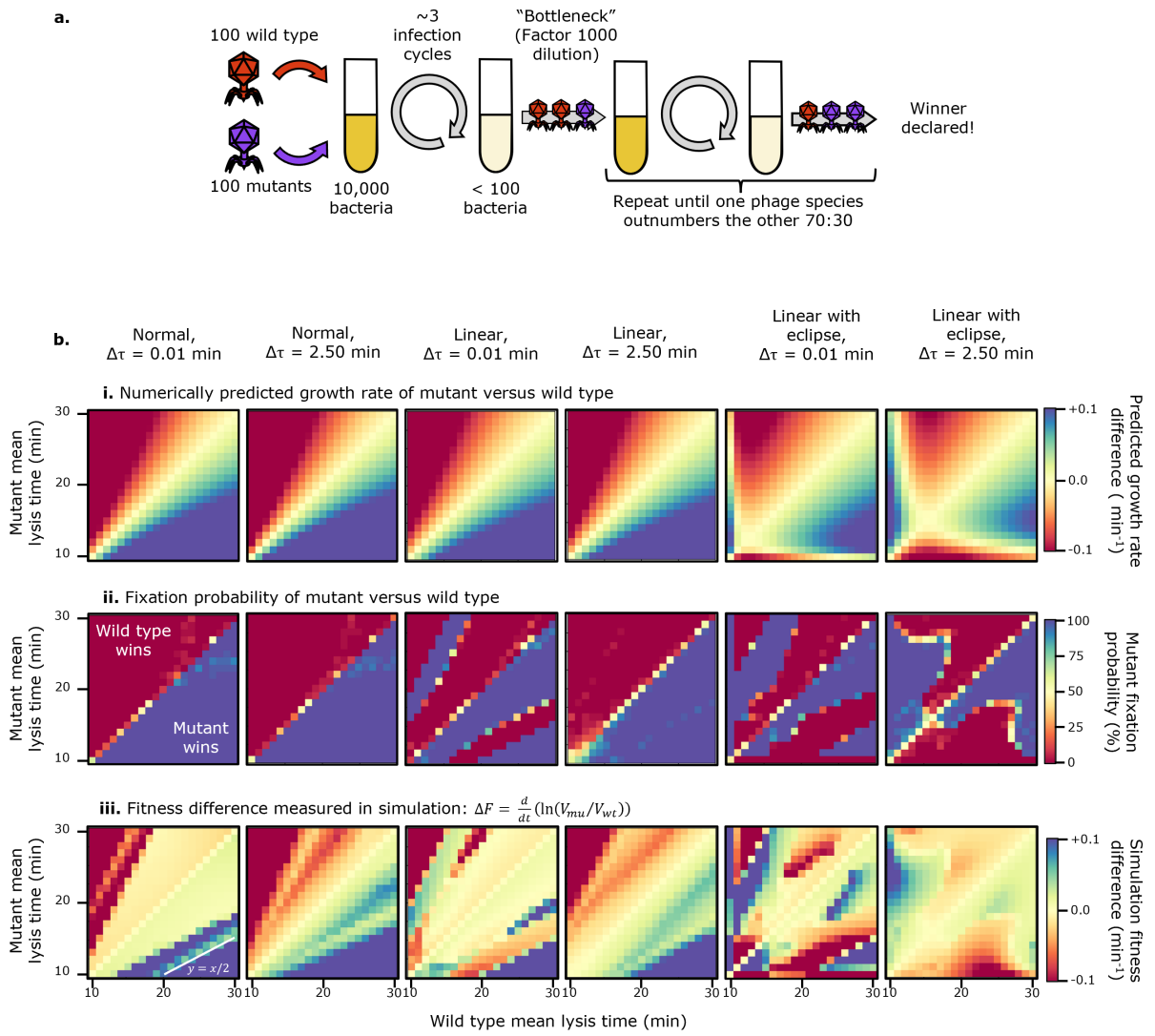

Figure 4: Results of serial passage competition experiment, competing a wild type against a mutant phage with different mean lysis times. **i.** Difference in numerically predicted growth rate, using equation 3. **ii.** Mutant fixation probability in stochastic simulation. **iii.** Fitness difference in stochastic simulation. Note that in the first and third rows, the visual scale has been set to saturate at ±0.1.

The third and fourth columns of Fig.4b correspond to the 'linear' model ($\beta = m'\tau$). When compared to the normal model, the principle difference is that the population resonance effect is stronger. The fixation probability plots (second row) show that, in the 0.01 min std case, population resonance is strong enough to flip which phage reaches fixation. In the 2.5 min case this is not true, as de-synchronisation in lysis cycles weakens the resonance effect, but slight deviations from 100% fixation are visible as a pale blue line in the otherwise uniform block of blue.

The reason why population resonance is stronger under the 'linear' model than under the 'normal' model is that in the 'linear' model longer lysis times confer larger bursts. Hence, while the faster-growing mutant is losing virions during the dead period, the slower-growing wild type benefits from a larger final burst. This longer lysis cycle and larger burst size would not be a winning strategy under exponential growth conditions, as shown in the theoretical expectation for the effective growth rate (top row). However, in the resource-limited conditions of a serial passage, forcing an opponent to lose virions to super-adsorption and decay while taking time to produce more offspring can be a winning strategy. This is in effect a weaponisation of a long lysis time.

Finally, the two rightmost columns on figure 4b correspond to the 'linear with eclipse' model ($\beta = m(\tau - \varepsilon)$). The topography of the fitness landscape is altered by the introduction of a critical point corresponding to

the optimum lysis time, visible in the top row as the intersection of two (yellow) contours of zero fitness difference and corresponding to the maxima identified in Fig. 3: earlier in the low std case, and shifted later in the higher std case. At the same time, the population resonance effect is here even stronger than under the 'linear' model, as longer lysis times imply even greater benefits in burst size.

The fixation probability and the fixation rate plots for the 2.5 min std case (middle and bottom rows, rightmost column) shows that the population resonance stripes are now impactful enough to remain present even with greater lysis time variation, and hence less synchronised lysis cycles, but are "rounded off" by the noise in lysis time. Indeed, a very similar shape can be obtained by applying a Gaussian blur to the corresponding plots in the 0.01 min std case.

In summary, our results reveal the presence of population resonance as a novel effect that arises when two bacteriophage populations in competitions are characterized by specific relative lysis times. It is strongest when lysis time is tightly distributed, and when longer lysis times lead to larger burst size. According to our simulations, population resonance allows one bacteriophage to outcompete another phage that would grow faster in isolation.

3.3 Serial passage experiments suggest lysis time noise is beneficial even at the cost of reduced growth rate

Having shown that noise in lysis time meaningfully affects which of two competing bacteriophage strains reaches fixation, we now explore whether variability in lysis time can be under selective pressure and quantify its direct effects on competitive fitness. We repeat the serial passage competition experiment described in section 3.2, keeping the wild type phage's mean lysis time and std constant (17 min and 2.5 min, respectively), while varying those of the mutant (Fig. 5).

The first two columns, corresponding to the 'normal' and 'linear' models, are qualitatively similar to each other. In both cases, the theoretical growth rate difference (top row) suggests that a mutant with a shorter lysis time should grow faster than the wild type. The yellow contour of equal fitness has a slightly positive gradient, meaning that a phage should see an equal gain in fitness by either reducing its mean lysis time by 1 minute, or increasing its lysis time std by approximately 3 minutes.

The middle row (fixation probability) agrees with the overall claim that shorter lysis times are advantageous, but the slope of the equal-fitness contour is higher than in the top row, suggesting that, under the resource-limited conditions of the serial passage, each 1 minute decrease in lysis time mean is competitively equivalent to an increase of approximately 1 min in lysis time std. Since this increase in gradient similarly holds for both the 'normal' and the 'linear' models, it cannot be understood in terms of the trade-off between lysis time and burst size characteristic of the latter, but it is the manifestation of an intrinsic benefit of stochasticity under resource-limited conditions.

An explanation for this result is the following. In exponential growth, one bacteriophage strain will outcompete the other if its growth rate is consistently higher, therefore its lysis cycles must be fast on average. In the serial passage experiment, bacteria are limited and vastly outnumbered by the phage towards the end of each passage (multiplicity of infection, MOI, approaching 100). Here, a bacteriophage strain does not need to have short lysis cycles on average, rather it needs enough short lysis cycles to secure a larger share of the available bacteria, which can be achieved with large variation around the mean.

The rate of fixation (bottom row) provides a finer quantification of these results, as we see that the mutant fitness disadvantage at high mean lysis times predicted by growth in isolation can be overcome by increasing lysis time std. For a given std, the fitness difference as a function of mean lysis time displays a non-monotic behaviour. This is a result of the population resonance effect described in the previous section. Importantly, while increasing noise slightly decreases the relative advantage emerging from the resonance effect, it also broadens the region of parameter space in which it is relevant (Fig. S13i).

The rightmost column of Fig. 5 corresponds to the 'linear with eclipse' model. Here, the numerical growth rate prediction (top row) points to a small optimal region of parameter space (short lysis time, low std, lime green) below and to the left of the equivalence point, in which the mutant should grow faster than the wild

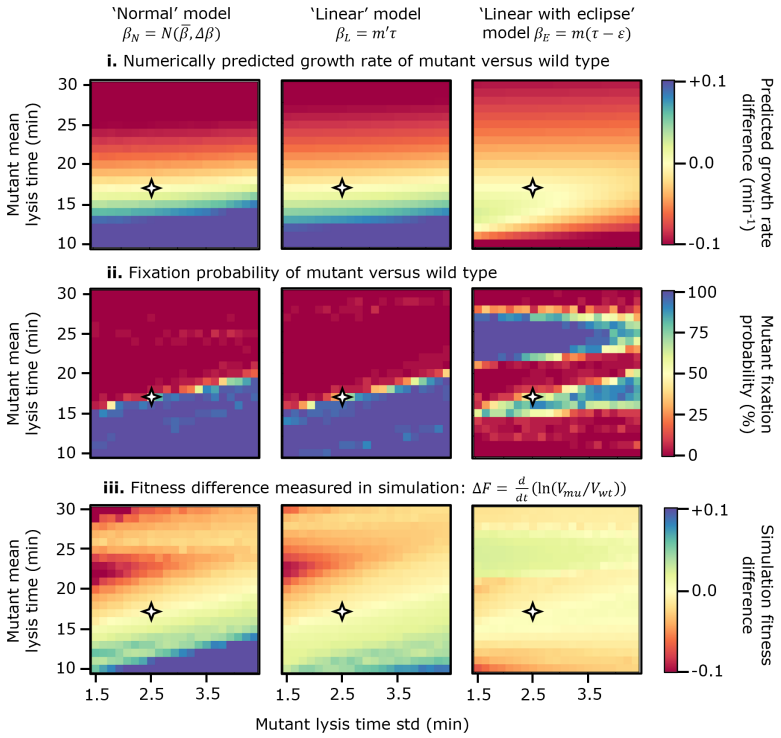

Figure 5: Results of serial passage competition experiment, where a wild type phage with lysis time mean 17 min, std 2.5 min competes against a mutant with varied lysis time mean (y-axis) and std (x-axis). **i.** Difference in numerically predicted growth rate, using equation 3. **ii.** Mutant fixation probability in stochastic simulation. **iii.** Fitness difference in stochastic simulation. Note that in the first and third rows, the visual scale has been set to saturate at ±0.1. Axes are scaled such that each pixel step in the y direction corresponds to a 1 minute change in mean lysis time, while each pixel step in the x direction corresponds to an equivalent fractional change in lysis time std versus the wild type value: 2.5/17 minutes. The four-point star on all panels correspond to the point in parameter space at which both phages have exactly the same parameters.

type. This reflects the finding in section 2.3, and the fact that the wild type phage is already quite close to the optimum. Interestingly, the mutant fixation probability plot (second row) shows a different picture, in which two distinct regions of parameter space result in mutant fixation. The region towards the top of the plot is the result of population resonance (when super-adsorption and decay are disabled this region disappears, Fig. S14).

The high-fitness region at the bottom of the plot, which in the other models extends to the x-axis, is here instead bounded due to the presence of the eclipse period: if the mean lysis time of the mutant is too close to the eclipse period, the mutant will not be competitive. This result agrees with numerical prediction (top row). The fitness difference in simulations, however, disagrees with numerical predictions in that the majority of this high fitness region is to the right of the equivalence point, rather than below and to the left. This is because, as mentioned previously, when resources are sufficiently limited that only a small number of lysis cycles are possible, the optimal strategy is not to maximise steady-state growth rate, but rather to carry out fast early lysis cycles, which secure a majority share of the available resources, followed by slower but more productive later lysis cycles. An intermediate mean lysis time and larger lysis time std make this possible. The lysis time std cannot be made too great, or the phage risks lysing before or shortly after the eclipse period, producing nothing. Hence, the lower edge of this high-fitness region is slightly upward sloped, favoring longer mean lysis times when the std is large.

In summary, we find that serial passage rewards lysis time variability more than numerical growth rate predictions would suggest. We reason that this is due to fast lysis cycles being disproportionately advantageous under resource-limited conditions as they ensure a greater share of the total, limited, pool of resources (bacteria). In the 'linear' and 'linear with eclipse' models, larger lysis time std allows for both shorter lysis cycles that produce virions quickly to claim the available resources, and longer, more productive later cycles that

generate more virions. It should be stressed that this winning strategy is achieved only probabilistically: an individual phage is equally likely to cause a faster-than-average first lysis cycle as to cause a slower-than-average cycle. If the phage could sense the culture MOI and 'decide' to lyse rapidly when MOI is low and slowly when MOI is high, such as through a lysis-inhibition mechanism [56], this would be an even more competitive strategy.

3.4 Plaque expansion assay does not exhibit population resonance and results in weaker selective pressure on lysis time

We now move to a second standard phage growth assay, a plaque expansion across a bacterial lawn, which we simulate as a one dimensional series of well-mixed demes (Fig. 6), as detailed in the Methods section. Free virions, but not bacteria, are able to diffuse between adjacent demes (Fig. 6a).

The data in the top row is identical to that in Fig. 5, with a different colour range to make it directly comparable with the data from the simulations of plaque expansions. For the 'normal' and 'linear' models, the results share some common features with the serial passage case. Particularly, the line of equal fitness has a steeper gradient in the stochastic simulation plot (second row) than the predicted growth rate plot (top row), suggesting that lysis time variation is still rewarded more strongly than its effect on growth rate alone should predict. This is not surprising, as the typical MOI in plaque expansion is very high, making resources even more limited.

The fitness difference plots (third row) are markedly different to those produced by serial passage. First, the population resonance effect is no longer present, since virions no longer experience a "dead period" waiting for new bacteria to be added. Secondly, fitness (dis)advantages are overall smaller in magnitude here than in the serial passage case. In particular, a mutant with a lysis time mean larger than the wild type's is able to persist for much longer and, vice-versa, a fast lysing mutant will take more time to fix.

The final row shows the infection wave's velocity, which is determined by the winning phage. A mutant which produces a much faster infection front will quickly overtake and outcompete the wild type phage. The white polygon corresponds to the region of parameter space in which the wild type phage reaches fixation, and therefore we expect the wave velocity to be constant. Mutants with shorter mean lysis times and greater lysis time std produce faster infection waves, but infection waves are significantly slower in the linear model (max roughly 6 μm/min) than in under normal model (max roughly 11 μm/min), as a result of the trade-off between lysis time and burst size.

The third column corresponds to the 'linear with eclipse' model. As in the serial passage experiment, the optimal region of parameter space in which the mutant is able to reach fixation (second row, green ellipse) is not located where the numerical growth rate would suggest (top row). Its shift towards high std values strongly supports the idea that lysis time noise is beneficial in resource-limited environments.

The third row (fitness difference) and fourth row (infection wave velocity) show a general loss of contrast across the majority of the parameter space. This suggests that when a strong trade-off between lysis time and burst size is present (second and third columns), the plaque expansion puts little (second column, 'linear' model) to almost no (third column, 'linear with eclipse' model) selective pressure on lysis time, as any benefit coming from lysing faster is compensated by the lower burst size.

In summary, a spatially structured environment removes any population resonance effect, and generally masks the selective pressure on lysis time compared to a serial passage setup. In line with this, we also find that noise in lysis time is overall less critical in determining phage fitness in a range expansion.

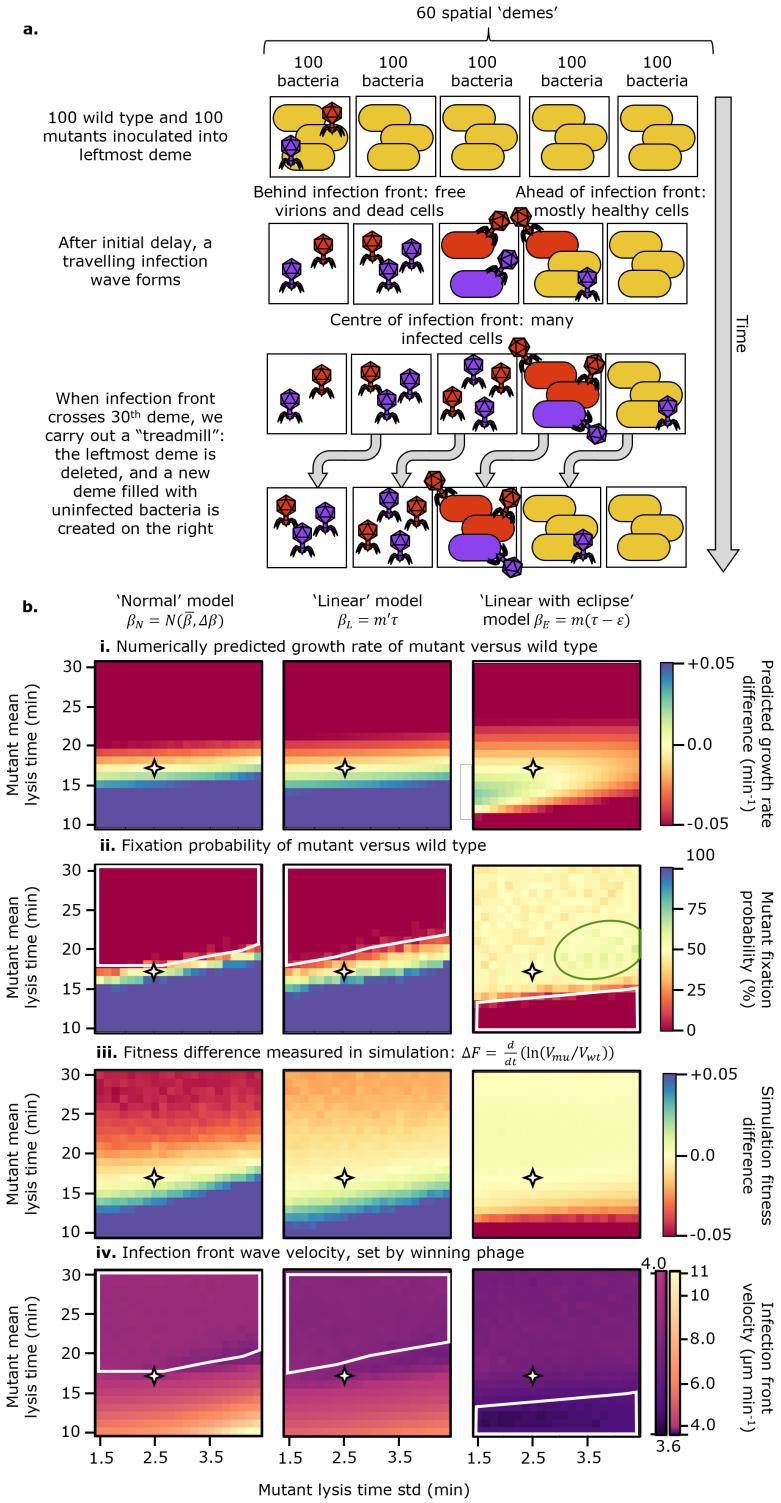

Figure 6: **a.** Plaque expansion experiment schematic. **b.** Results of plaque expansion competition experiment, where a wild type phage with lysis time mean 17 min, std 2.5 min competes against a mutant with varied lysis time mean (y-axis) and std (x-axis). **i.** Difference in numerically predicted growth rate, using equation 3. **ii.** Mutant fixation probability in stochastic simulation. **iii.** Fitness difference in stochastic simulation. **iv.** Infection front velocity. Note that in the first and third rows, the visual scale has been set to saturate at ±0.05. Axes are scaled such that each pixel step in the y direction corresponds to a 1 minute change in mean lysis time, while each pixel step in the x direction corresponds to an equivalent fractional change in lysis time std versus the wild type value: 2.5/17 minutes. The four-point star on all panels corresponds to the point in parameter space at which both phages have exactly the same parameters. The white polygons in rows ii and iv outline the parameter space in which the wild type reaches fixation.

4 Discussion

Clonal bacteria growing under identical conditions display significant heterogeneity in gene expression due to intrinsic biochemical noise [29]. It is therefore expected that bacteriophages, which heavily rely on their host's molecular machinery, are subject to similar unavoidable stochasticity in their replication. The extent and pervasiveness of such noise in a phage's life history parameters cannot be measured by traditional phenotypic assays based on bulk population measurements, and as such, they have remained inaccessible until recently [12, 37]. As a result, the vast majority of experimental and theoretical work aimed at quantifying phage ecology and evolution has focused on fitness effects linked to average values. Recent advances in single-cell measurements of phage-bacteria interactions [12, 37] and more careful analyses of population assays [11] are finally enabling an experimental quantification of variability in life history parameters, raising the question of whether noise can be a beneficial inheritable trait for a phage population.

In this work, using extensive agent-based simulations, we have investigated how phenotypic stochasticity in lysis time and burst size can confer fitness (dis)advantages to a phage population in two commonly used experimental assays: serial passage and plaque expansion. Overall, our results indicate that variability is generally an advantageous trait, even when phage production rate alone would predict the opposite. Interestingly, the origin of this advantage intimately depends on both the phage propagation assay (serial passage vs. plaque expansion) and the specific biological trade-off between lysis time and burst size.

Across our different scenarios, we find that a powerful selector for phenotypic variability is resource limitation. Most laboratory settings, and likely wild environments, are characterized by periods of time or regions of space with very high MOI, where many phage virions compete for few host cells. In these conditions, noise in lysis time appears to confer increased resilience to a phage population. By producing virions throughout time and not in synchronized large bursts, variable lysis times can establish a more steady flow of virions, so that susceptible cells can be infected whenever and wherever they become available. This effect becomes crucial when free virions are subject to rapid loss, e.g., because of super-adsorption. Importantly, while a low adsorption rate also desynchronises virion release, it inevitably reduces growth rate because of the time spent searching a host (see predicted growth rates in Fig. 4 vs Fig. S9). Reduced adsorption rate may still be beneficial if prolonged periods of very high MOI are common, since it reduces a bacteriophage's chance to be wasted through super-adsorption, but it would come at the cost of slowing down infection when susceptible cells do become available.

One of the fundamental differences between noise in division time in bacteria and noise in lysis time in phages is the trade-off between the length of the latent period τ and the burst size β (unlike for bacteria, which will always replicate into two daughter cells upon division). Our results show that the details of this trade-off have strong influence on the fitness landscape of the phage and on how noise modulates it. Surprisingly, a linear correlation between burst size and lysis time results in a fitness map that is very similar to the one generated in the absence of any trade-off, both in serial passage and in plaque expansion scenarios. In all these situations, we find a strong selection towards fast lysis cycles, whether this occurs by decreasing the mean lysis time, or by increasing the variability in lysis time so that more infection cycles are completed rapidly.

For an optimal lysis time to emerge, a non-productive eclipse period has to be introduced in the trade-off. In this case, we find that serial passage and a plaque expansion competition lead to very different selective pressures on the phage. In the former, fitness favours two opposite strategies: "patient" and "rapacious". The "patient" strategy uses a relatively slow mean lysis time with little variability, so that the phage can exploit the population resonance effect and effectively "outlive" the competing faster-lysing phage. The "rapacious" strategy favors shorter lysis time with high variability, so that the phage quickly removes potential host cells for the slower lysing competing phage and relies on the occasional longer cycles for productive infections. Both the "rapacious" and the "patient" strategies are able to outcompete a "prudent" strategy based on maximising growth rate in isolation (intermediate mean lysis time, very small std) because of the competition for limited resources (cells) between two phage populations. The efficacy of a similarly rapacious strategy was observed in [57], in which a fast-migrating, fast-lysing phage was able to out-compete a slower-lysing prudent phage, which grew more quickly in isolation.

It would be interesting to test experimentally which strategy would actually preferentially emerge in an evolutionary experiment. While the outcome will be sensitive to the availability of mutations and potential epista-

sis, we expect that the rapacious strategy (short lysis, large variability) will typically be more robust, since the presence and location of population resonance, which is leveraged by the patient strategy, strongly depends on the details of the competing phage, the number of cells at the beginning of each serial passage, and the initial MOI (see Figs. S8, S12, S14).

Unexpectedly, we find that introducing an eclipse period in the lysis time-burst size trade-off almost completely flattens the fitness landscape when phages compete in a plaque expansion, as long as lysis time is larger than the eclipse period. This result implies that there should be almost no selective pressure on lysis time or its variability in an evolutionary experiment performed on a bacterial lawn, possibly explaining why several studies performing such experiments predominantly find mutations related to adsorption [57, 58]. Interestingly, our finding also suggests an indirect way to identify the presence of a strong trade-off between burst size and lysis time. A plaque assay competition dominated by fast-lysing phages would indicate the absence of a strong trade-off. In contrast, a plaque competition dominated by slow, highly productive phages could indicate the presence of a strong trade-off between lysis time and burst size, and, likely, the presence of a strongly conserved eclipse period.

Can variability in lysis time be an adapted trait? When no or minimal trade-off between lysis time and burst size exist, our results show that selection will simply push the phage to lyse as quickly as possible. In this case, noisy phages could potentially emerge only if there is a lower limit to how short a deterministic lysis time can be or if it is evolutionary easier, because of availability of mutations or presence of epistatic effects, to increase variance in lysis time rather than decreasing its mean. However, in the presence of an eclipse period, an optimal lysis time value exists. Once the phage reaches this optimum, we expect that the selective pressure will concentrate on optimizing variability in lysis time. Experimentally testing these hypotheses will not only clarify the evolutionary role of noise in phage ecology and evolution, but also reveal which genetic changes can modulate variability in lysis time. We speculate that some of these mutations could achieve such goal by harnessing the intrinsic noise of the host cell, and provide a deeper understanding of the intricate interplay between an infecting phage and its host.

5 Data availability

The stochastic, agent-based simulation "Stochastic 3.3.2" was written in Python 3, based on earlier computational work [30]. Simulations were executed on the CSD3 high performance computing cluster at University of Cambridge. The code used for the full simulation, minimal "fast" simulation, numerical integration and heat-map plotting is available at `https://github.com/FuscoLab/lysis_time_noise`.

6 Acknowledgements

AS and DF were supported by an ERC Starting Grant/UKRI Horizon Europe Guarantee (EP/Y030141/1). MH was supported by a UKRI EPSRC Doctoral Studentship from the Department of Physics, University of Cambridge (2125180). Simulations in this work were performed using resources provided by the Cambridge Service for Data Driven Discovery (CSD3) operated by the University of Cambridge Research Computing Service (`www.csd3.cam.ac.uk`), provided by Dell EMC and Intel using Tier-2 funding from the Engineering and Physical Sciences Research Council (capital grant EP/T022159/1), and DiRAC funding from the Science and Technology Facilities Council (`www.dirac.ac.uk`).

7 Supplementary

7.1 Single phage killing curve simulation suggests variability in burst size alone has little to no effect on bacteriophage fitness

We ran a preliminary simulation to investigate the effects of variability in burst size and lysis time on a single phage species' ability to clear a bacteria culture. We simulate a protocol which we name the "killing curve": 100 bacteriophages are introduced to a growing bacterial culture, volume 10^{-5}ml, carrying initially 10,000 cells (carrying capacity 100,000). The infection is allowed to proceed until the number of bacteria drops below 100 (1% of its initial value). We record the time taken for this to occur (T_{100}), the maximum count of living bacteria observed ($B_{\max}$), and the number of phages remaining at the end (V_{end}). We then calculate an effective production rate, (r) for the bacteriophage through $r = V_{\text{end}}/T_{100}$.

This simulation is similar to the serial passage simulation discussed in section 3.2 except that only one phage strain was used and there was no transfer to a new culture. The simulation was used to investigate six possible models:

(i) 'All constant', in which τ and β are both completely fixed and deterministic.

(ii) 'Burst size varied', in which τ is fixed and β is drawn from a normal distribution.

(iii) 'Lysis time varied', in which τ is drawn from a normal distribution and β is fixed.

(iv) 'Normal model', in which τ and β are both drawn from uncorrelated normal distributions.

(v) 'Linear model', in which τ is drawn from a normal distribution and β is calculated via $\beta = m'\tau$.

(vi) 'Linear with eclipse model', in which τ is drawn from a normal distribution and β is calculated via $\beta = m(\tau - \varepsilon)$.

Models (iv) through (vi) being those used in the main paper. All parameters used were the same as in serial passage simulations, and can be found in tables 2 to 5. In each case, the simulation was run 20 times and the results were averaged. The simulation was then run an additional 20 times for each model under "conservative" conditions, in which phages did not decay, and only a single phage could bind to each cell.

Figure S1a shows example population dynamics for each burst size model. In all cases the bacterial culture is eradicated in 3 rounds of lysis lasting approximately 17 minutes each. The models which include variable lysis time produce smoother population curves, while the models with deterministic lysis time produce sudden jumps.

The averaged results over 20 simulations (Fig S1b) suggest the following. Variability in lysis time leads to faster bacterial eradication (Fig S1bi). This allows the bacteria less time to divide, reducing the number of available cells (Fig S1bii), and therefore the number of phage produced (Fig S1biii). Hence, variability in lysis time leads to a greater production rate of phages (Fig S1biv) but fewer phages in total.

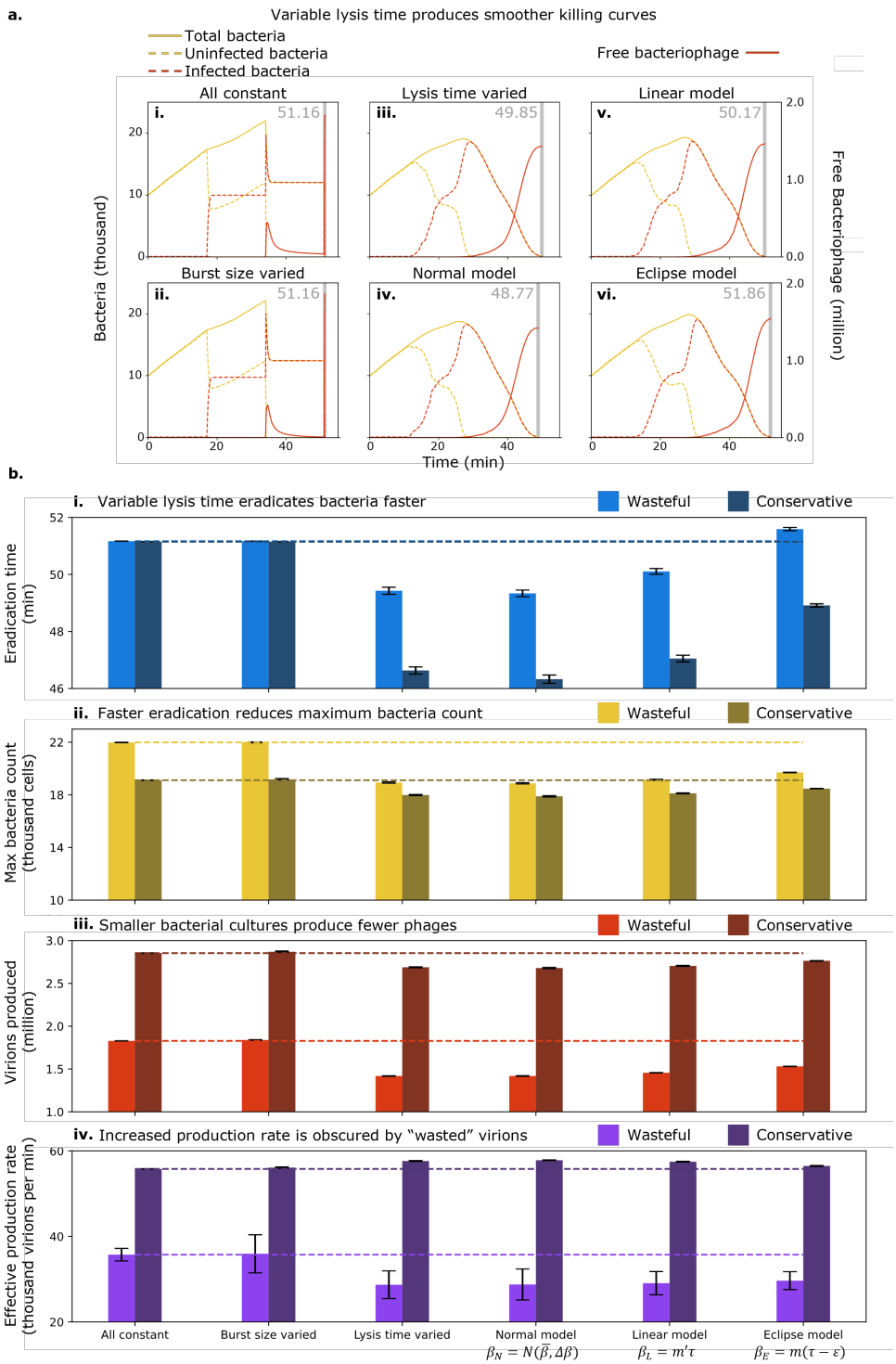

Fig. S1: **a.** Example population curves for the six models tested. The grey vertical line in each panel shows the time at which 99% eradication was achieved and the simulation was terminated. **b.** Results averaged over 20 killing curve simulations showing **i.** Time to 99% eradication,**ii.** Maximum cell count, **iii.** Total virions at time of eradication, **iv.** Virions produced per minute. Error bars show the standard error in the mean.

We also note the significant difference between the "wasteful" and "conservative" cases, and the lack of meaningful difference between the "all constant" and "burst size varied" models, or separately between the "lysis time varied" and "normal" models. While, analytically, we may expect variation in burst size to slightly reduce growth rate (the growth rate $k = \ln(\beta)/\tau$ is concave in β), under these conditions the MOI quickly becomes much greater than 1 and the laws of exponential growth cease to apply.

In summary, variability in burst size seems to have little to no effect on a phage's ability to eradicate cells or proliferate itself. Lysis time variability however seems to hasten cell culture eradication, at the inevitable cost of fewer virions being produced, as there are fewer cells to consume.

7.2 Derivation of fitness difference ΔF

Consider two populations, P_1 and P_2, growing exponentially at rates k_1 and k_2, such that

$$P_1(t) = P_1(0)e^{k_1 t}$$

and

$$P_2(t) = P_2(0)e^{k_2 t}$$

taking the ratio of these populations at time t,

$$\frac{P_2(t)}{P_1(t)} = \frac{P_2(0)}{P_1(0)} e^{(k_2-k_1)t}$$

then taking the natural logarithm of that ratio,

$$\ln\left(\frac{P_2(t)}{P_1(t)}\right) = \ln\left(\frac{P_2(0)}{P_1(0)} e^{(k_2-k_1)t}\right) = \underbrace{\ln\left(\frac{P_2(0)}{P_1(0)}\right)}_{\text{constant}} + (k_2-k_1)t$$

finally, differentiating with respect to time,

$$\frac{\mathrm{d}}{\mathrm{dt}}\left(\ln\left(\frac{P_2(t)}{P_1(t)}\right)\right) = k_2 - k_1 := \Delta F$$

To avoid ambiguity, we use k to refer to growth rates predicted by numerical integration, and ΔF to refer to fitness differences measured in the agent based simulation.

If we now consider bacteriophage populations specifically, note that here, P_i must refer to the total population of all virions of type i, including those adsorbed to cells. Under the assumptions made, specifically instantaneous adsorption, no super-adsorption, and infinitely abundant bacteria, all phages will be uniquely adsorbed to a cell, hence an equivalent expression for ΔF is

$$\Delta F_I := \frac{\mathrm{d}}{\mathrm{dt}}\left(\ln\left(\frac{I_2(t)}{I_1(t)}\right)\right).$$

This quantity also works as a measure of fitness difference in resource-limited conditions, because, as one phage grows in population relative to the other and approaches fixation, the ratio of infected cells will converge to 0 or 1.

An alternate expression for ΔF is

$$\Delta F_V := \frac{\mathrm{d}}{\mathrm{dt}}\left(\ln\left(\frac{V_2(t)}{V_1(t)}\right)\right),$$

which uses the ratio of free virions V_2/V_1, as opposed to all virions P_2/P_1. This quantity cannot be continuously evaluated as free phage populations frequently fall to zero, so must be evaluated only when it is meaningful, such as right before the transfer step of a serial passage. The ΔF_V definition does, however, have the advantage that adsorbed phages, which are functionally dead for reproductive purposes, no longer contribute to the fitness. For an analysis of these two possible fitness definitions, see section 7.4.1 and Fig S6. In the main paper we employ ΔF_V for serial passage simulations, and ΔF_I for plaque expansions.

7.3 Asymmetric and symmetric lysis time distributions exhibit the same qualitative behaviour

7.3.1 Erlang distribution

The Erlang distribution is a natural choice for consideration due to its biological relevance: it describes the time taken to complete a series of n exponential processes, each occurring at rate λ.

$$p(\tau) = \frac{\lambda^k \tau^{k-1} e^{-\lambda\tau}}{(k-1)!} \tag{5}$$

We parametrise our Erlang distribution using the shape n and mean $\overline{\tau} = n/\lambda$. In agreement with Fig 3, under the 'normal' and 'linear' models, for a given mean lysis time, a greater variability (which in the Erlang distribution corresponds to smaller 'shape' n) is preferred. Under the 'eclipse' model, a tighter distribution (larger shape) is preferred.

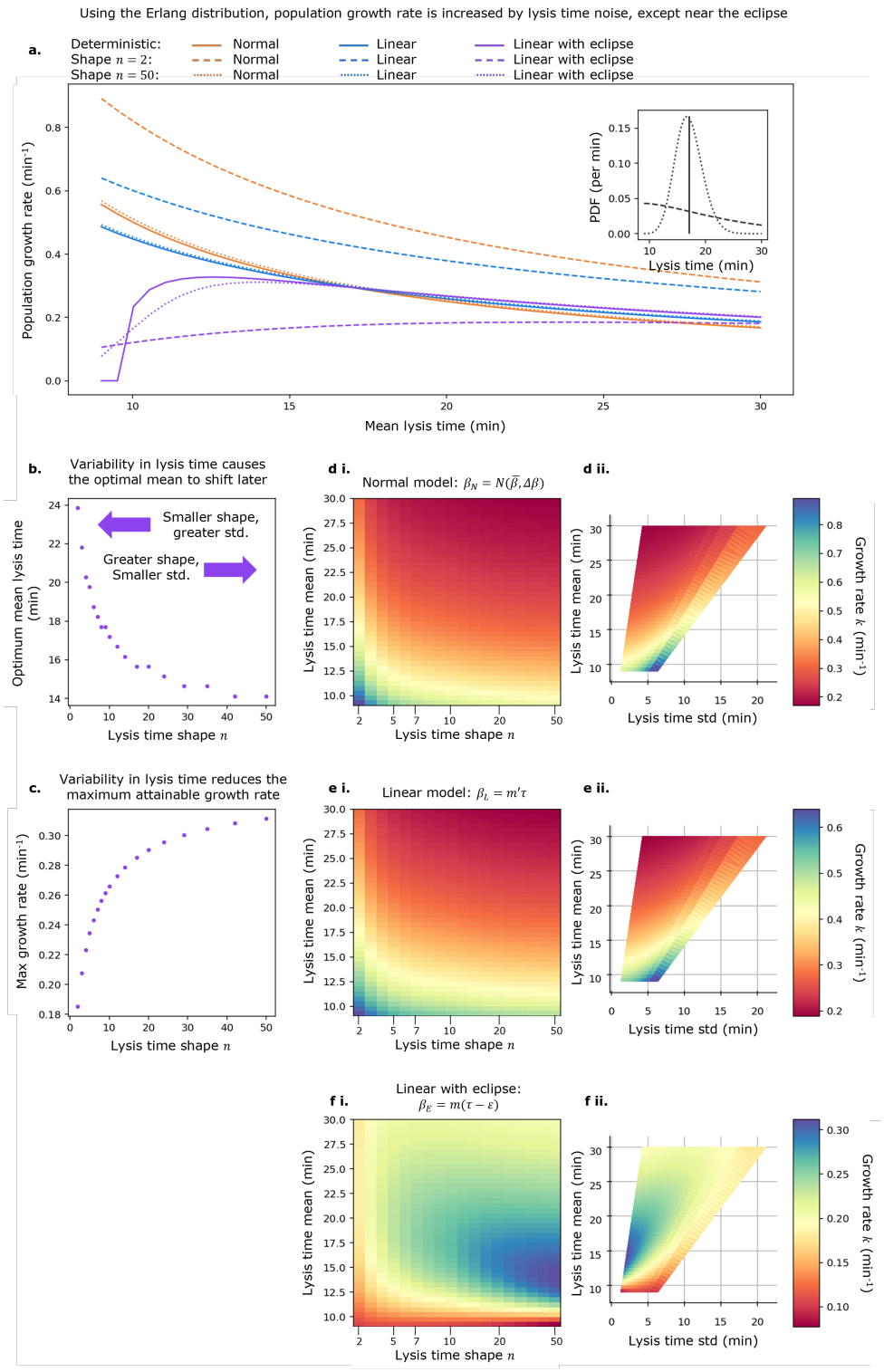

Fig. S2: **a.** Bacteriophage effective growth rate k as a function of mean lysis time, for either totally deterministic lysis time (solid lines), Erlang distributed lysis time with shape 2 (dashed lines), or shape 50 (dotted lines). Inset: example lysis time distributions with mean 17 minutes: deterministic (solid line), Erlang with shape 2 (dashed line), Erlang with shape 50 (dotted line). **b.** Optimal lysis time under 'linear with eclipse' model as a function of lysis time shape n. **c.** Effective growth rate achieved at optimal lysis time, under 'linear with eclipse' model, as a function of lysis time shape. **d.** to **f.** Effective growth rate as a function of both mean lysis time and lysis time shape n for 'normal', ''linear', and 'linear with eclipse' models respectively (i), and the same data mapped to the lysis time mean and lysis time std axes (ii) to allow easier comparison with Fig 3.

7.3.2 Weibull distribution

The Weibull distribution usually represents 'time-to-failure', and is described by shape n ($1/n$ is approximately equal to the coefficient of variation) and scale λ.

$$p(\tau) = \frac{n}{\lambda} \frac{\tau^{n-1}}{\lambda} e^{-(\tau/\lambda)^n} \tag{6}$$

In agreement with Fig. 3, under the 'normal' and 'linear' models, for a given mean lysis time, a greater variability (which in the Weibull distribution corresponds to smaller shape n) is preferred. Under the 'eclipse' model, a tighter distribution (larger shape) is preferred.

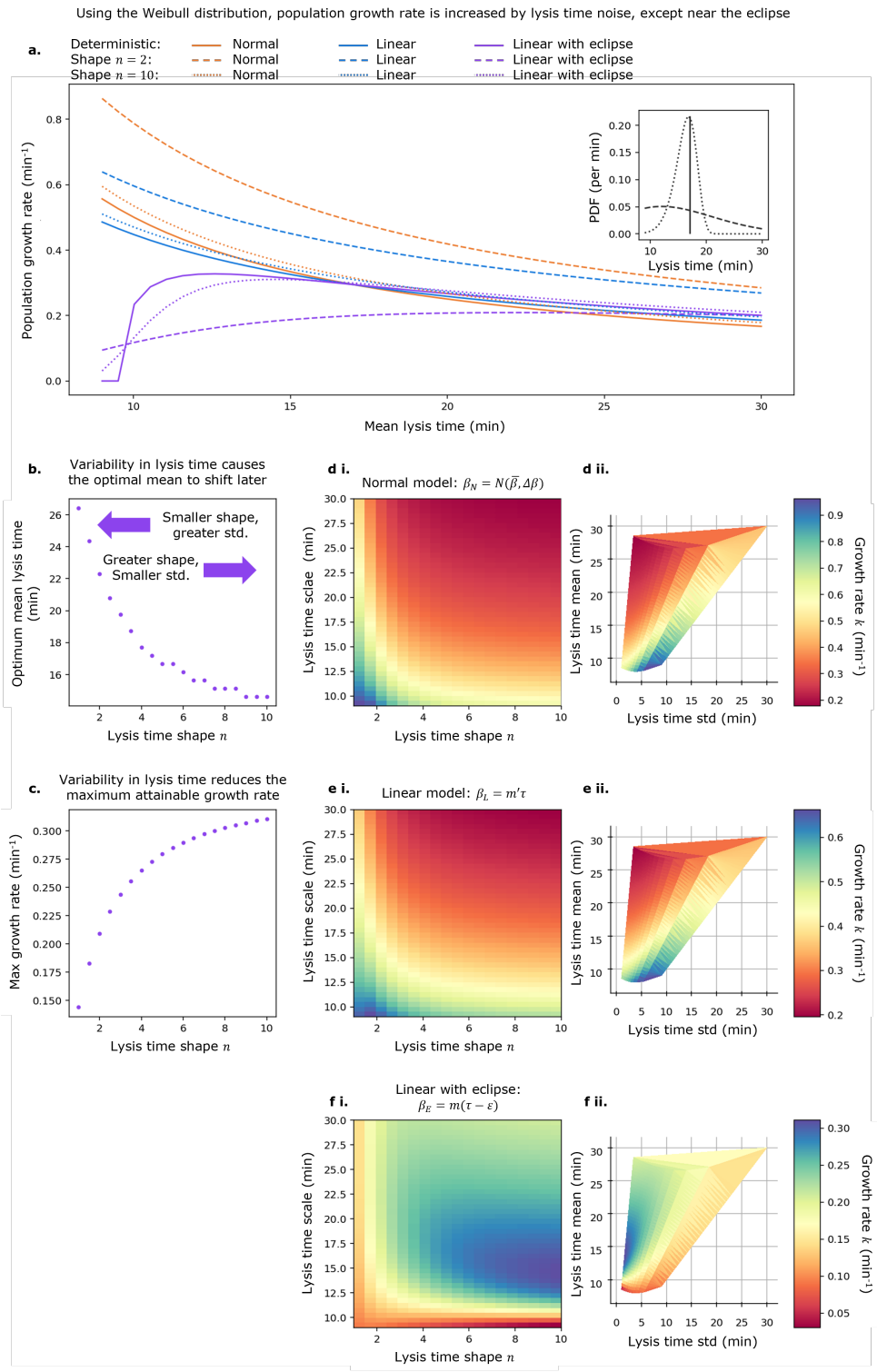

Fig. S3: **a.** Bacteriophage effective growth rate k as a function of mean lysis time, for either totally deterministic lysis time (solid lines), Weibull distributed lysis time with shape 2 (dashed lines), or shape 10 (dotted lines). Inset: example lysis time distributions with mean 17 minutes: deterministic (solid line), Weibull with shape 2 (dashed line), Weibull with shape 10 (dotted line). **b.** Optimal lysis time under 'linear with eclipse' model as a function of lysis time shape n. **c.** Effective growth rate achieved at optimal lysis time, under 'linear with eclipse' model, as a function of lysis time shape. **d.** to **f.** Effective growth rate as a function of both mean lysis time and lysis time shape n for 'normal', ''linear', and 'linear with eclipse' models respectively (i), and the same data mapped to the lysis time mean and lysis time std axes (ii) to allow easier comparison with Fig 3.

7.3.3 Skew normal distribution

The skew normal distribution allows us to investigate the effects of skew explicitly. It is described by location μ, size σ and skew parameter α, and given by:

$$P(\tau) = \frac{2}{\sigma} p_N\left(\frac{x-\mu}{\sigma}\right) \times c_N\left(\alpha \frac{x-\mu}{\sigma}\right), \tag{7}$$

in which P_N and C_N correspond to the standard normal distribution's PDF and CDF respectively.

Defining the quantity δ as

$$\delta = \frac{\alpha}{\sqrt{1+\alpha^2}},$$

the skew-normal has true mean

$$\overline{\tau} = \mu + \sigma\delta\sqrt{\frac{2}{\pi}},$$

and true variance

$$(\Delta\tau)^2 = \sigma^2\left(1 - \frac{2\delta^2}{\pi}\right).$$

Which can be inverted to define the skew-normal instead through it's true mean, true std and parameter α via

$$\sigma^2 = (\Delta\tau)^2\left(1 - \frac{2\delta^2}{\pi}\right)^{-1},$$

$$\mu = \overline{\tau} - \sigma\delta\sqrt{\frac{2}{\pi}},$$

which is the parametrisation used in this investigation. True skew increases monotonically, though not linearly, with increasing α, and is zero at $\alpha = 0$.

We begin by fixing the lysis time std at 2.5 minutes and varying the mean and α.

For given mean lysis time, we find that growth rate k depends only weakly on skew. the 'normal' and 'linear' models show increased k for negative skew since this provides a greater likelihood of lysis events happening in near-zero time, which increases effective growth rate. The 'linear with eclipse' model shows a distinct and interesting result: at the lysis time which would be optimal in the totally deterministic case (in which the "distribution" reduces to a delta function) the growth rate obtained is equal for any value of α. At lysis times just longer than this optimum positive skew increases growth rate, while just shorter than the optimum negative skew increases growth rate.

Noting (i) that a positively skewed distribution has a steep left face, (ii) that a negatively skewed distribution has a gradually sloping left face and (iii) there is a "cliff edge" in the fitness landscape, in that lysis times below or close to the eclipse period (9.5 minutes) are extremely unproductive, we propose the following: starting with a longer value of lysis time and moving to shorter values, initially the cliff edge can be avoided by utilising a positively skewed distribution with a steep left face, ensuring almost no probability mass is to the left of the

cliff edge. As the mean gets closer to the cliff edge, this is no longer possible, so the optimal strategy instead is to switch to a strongly negatively skewed distribution, keeping the peak (mode) to the right of the cliff edge.

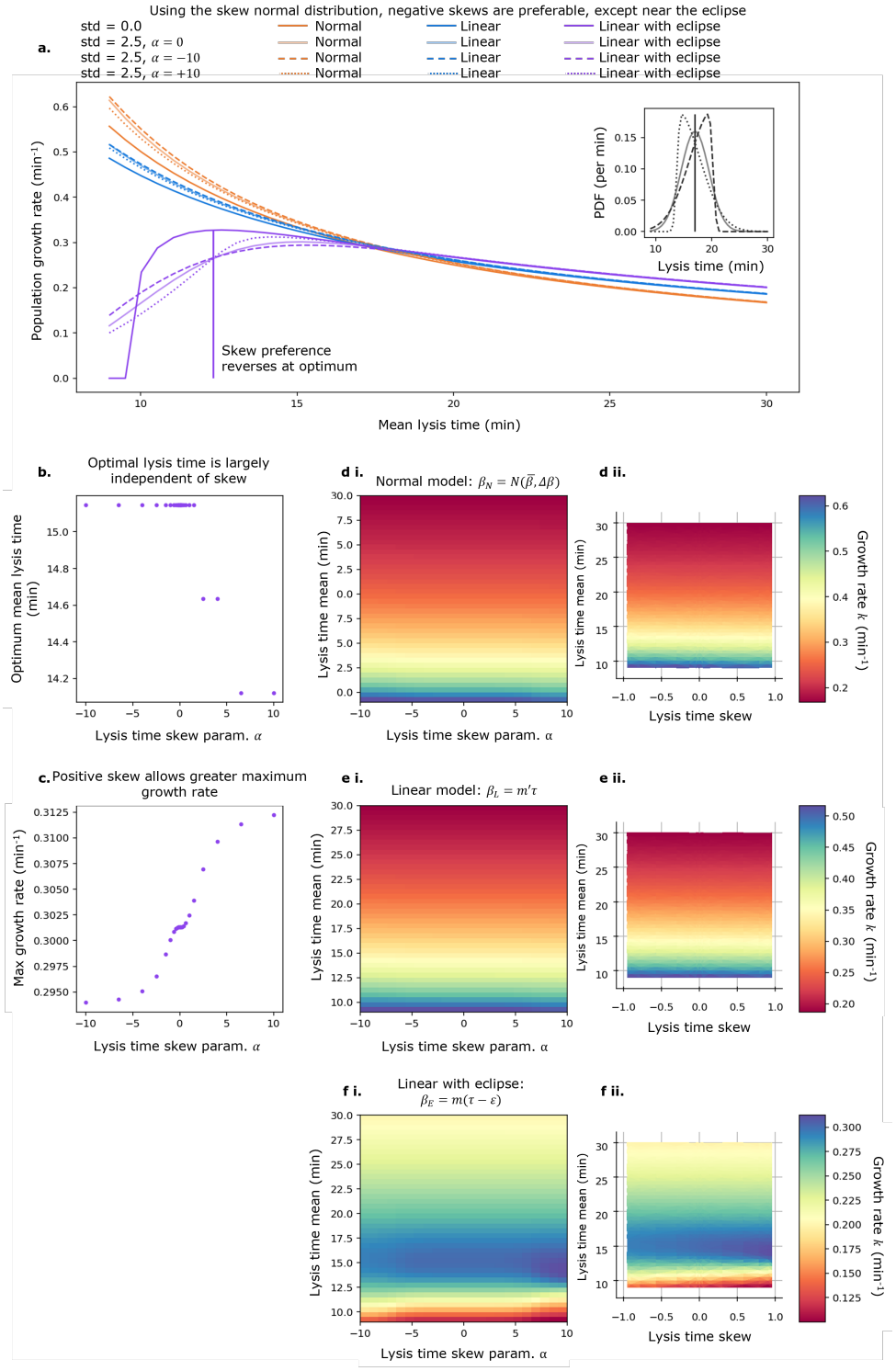

Fig. S4: **a.** Bacteriophage effective growth rate k as a function of mean lysis time, for either totally deterministic lysis time (solid lines), skew-normal distributed lysis time with lysis time std = 2.5 min and skew parameter $\alpha = 0$ (pale solid lines), $\alpha = -10$ (strong negative skew, dashed lines), or $\alpha = +10$ (strong positive skew, dotted lines). Inset: example lysis time distributions with mean 17 minutes: deterministic (solid line), skew-normal std = 2.5 min and skew parameter $\alpha = 0$ (pale solid lines), $\alpha = -10$ (dashed lines), or $\alpha = +10$ (dotted lines). **b.** Optimal lysis time under 'linear with eclipse' model as a function of skew parameter α. **c.** Effective growth rate achieved at optimal lysis time, under 'linear with eclipse' model, as a function of skew parameter α. **d.** to **f.** Effective growth rate as a function of both mean lysis time and skew parameter α for 'normal', ''linear', and 'linear with eclipse' models respectively (i), and the same data mapped to the lysis time mean and true statistical skew axes (ii) to compensate for non-linear relationship between α and true statistical skew.

Next, we fix the mean lysis time at 17 minutes, and vary the std and α.

As expected, the 'normal' and 'linear' models show the greatest increase in growth rate for large stds and negative skews. The 'linear with eclipse' model (at the 17 minute mean lysis time chosen) shows the greatest increase for intermediate std and positive skew. This is because 17 minutes is within the convex region of the growth rate function. The curvature,

$$\frac{d^2k}{d\tau^2} = \frac{d^2}{d\tau^2}\left(\frac{\ln(m(\tau-\varepsilon))}{\tau}\right) = \frac{2\ln(m(\tau-\varepsilon)) + \frac{\tau(2\varepsilon - e\tau)}{(\tau-\varepsilon)^2}}{\tau^3},$$

is positive for $\tau \geq 16.75$ minutes.

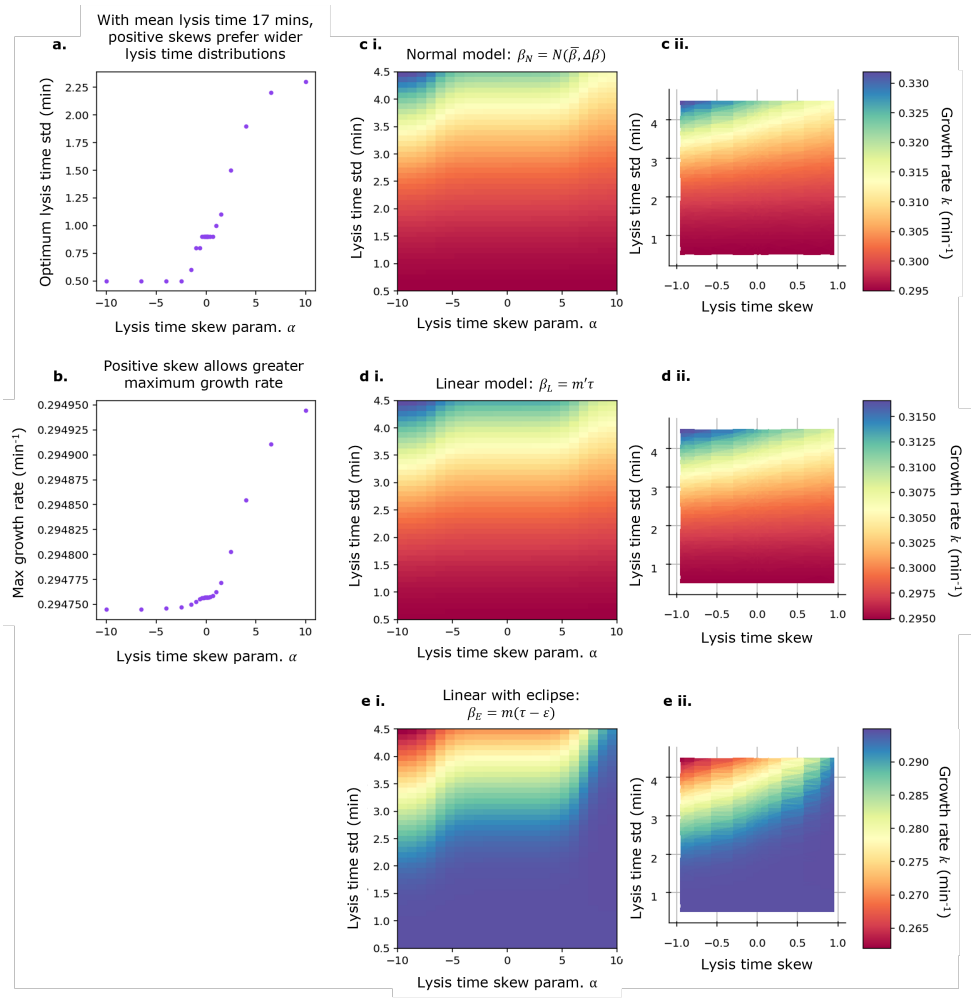

Fig. S5: **a.** Optimal lysis time std under 'linear with eclipse' model as a function of skew parameter α. **b.** Effective growth rate achieved at optimal std, under 'linear with eclipse' model, as a function of skew parameter α. **c.** to **e.** Effective growth rate as a function of both lysis time std and skew parameter α for 'normal', ''linear', and 'linear with eclipse' models respectively (i), and the same data mapped to the lysis time std and true statistical skew axes (ii) to compensate for non-linear relationship between α and true statistical skew.

7.4 Mean-mean serial passage controls

7.4.1 Fitness difference can be calculated through virion abundance or number of cells infected

In section 7.2, we describe how the fitness difference in simulation ΔF can be calculated using either the total free phage

$$\Delta F_V = \frac{\mathrm{d}}{\mathrm{d}t}\left(\ln\left(\frac{V_{\mathrm{mu}}}{V_{\mathrm{wt}}}\right)\right),$$

derived in 7.2, or using the number of infected cells

$$\Delta F_I = \frac{\mathrm{d}}{\mathrm{d}t}\left(\ln\left(\frac{I_{\mathrm{mu}}}{I_{\mathrm{wt}}}\right)\right).$$

In the main paper, we use the ΔF_V definition for serial passage simulations. In plaque expansion simulations, however, the 'treadmill' operation removes virions from the back of the travelling infection wave, so the quantities V_{wt} and V_{mu} are not meaningful away from the wavefront. We therefore use the ΔF_I definition.

To compare these definitions of ΔF, we present both here for the serial passage experiment described in Fig 4. In serial passage, both quantities are well defined, though not necessarily equivalent, if measured just before the transfer step. V_{mu} is the number of mutant virions remaining at time of transfer, and I_{mu} is the total number of cells infected by the mutant in the current passage cycle.

We see that the two definitions broadly agree, except that some features on the ΔF_V plots are not captured by the the ΔF_I plots (Fig S6 iii and iv). ΔF_V seems to be the better metric, in that it everywhere agrees with the mutant fixation probability. Disagreements seem mostly localised to the fitness "stripes", and are most pronounced under the 'linear' and 'linear with eclipse' models. The rationale for this is as follows. First, stripes represent regions where adsorption and decay shape the fitness landscape more than growth rate, hence ΔF_I may predict a phage should win as it infected more cells, but ΔF_V may capture that many of those virions then decayed. Second, these stripes are some distance from the line $y = x$, so, under the 'linear' and 'linear with eclipse' models, in which the stripes are more prominent, the disparity in lysis times and therefore burst sizes means there may be a significant difference in the ratios $V_{\mathrm{mu}}/V_{\mathrm{wt}}$ and $I_{\mathrm{mu}}/I_{\mathrm{wt}}$.

Because ΔF_V captures more features of the fitness landscape and better agrees with mutant fixation probability, this is the metric used in serial passage simulations.

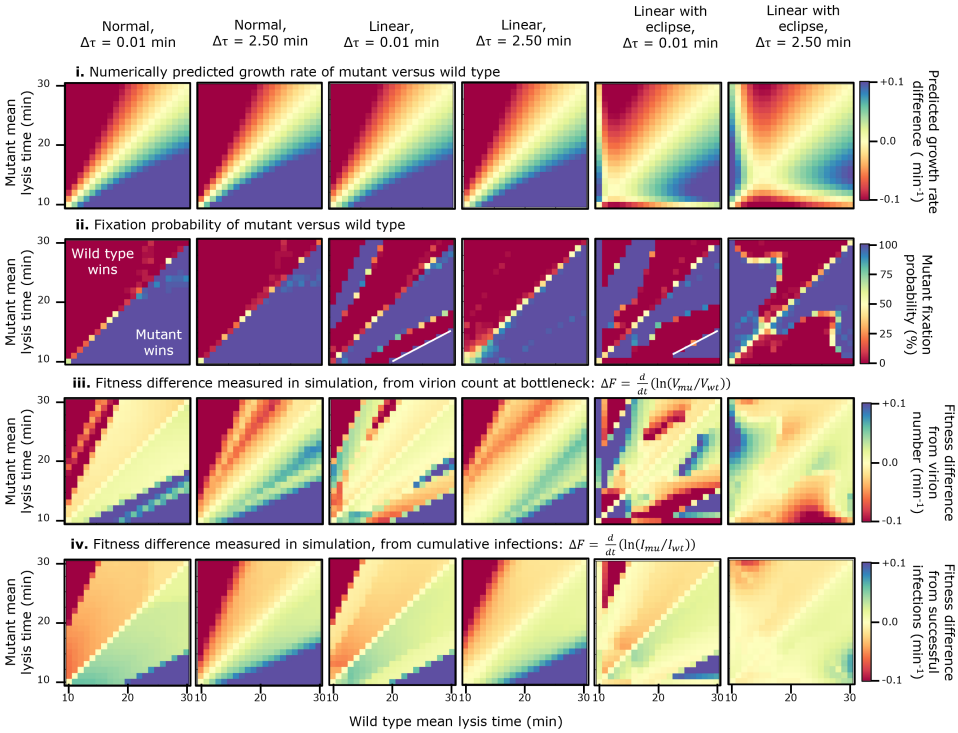

Fig. S6: Results of serial passage competition experiment, competing a wild type phage with one mean lysis time against a mutant with another. **i.** Difference in numerically predicted growth rate, using equation 3. **ii.** Mutant fixation probability in stochastic simulation. **iii.** fitness difference defined as $\Delta F_V = \frac{\mathrm{d}}{\mathrm{dt}}\left(\ln\left(\frac{V_{\mathrm{mu}}}{V_{\mathrm{wt}}}\right)\right)$. **iv.** fitness difference defined as $\Delta F_I = \frac{\mathrm{d}}{\mathrm{dt}}\left(\ln\left(\frac{I_{\mathrm{mu}}}{I_{\mathrm{wt}}}\right)\right)$.. Rows i to iii are identical to those in Fig 4.

7.4.2 Population resonance creates fitness "stripes"

To demonstrate the mechanism that gives rise to the observed "stripes" on the serial passage fitness landscape, we present example population traces from within and just to the right of the stripe for each of the three burst size models Fig S7a. In all cases the mutant phage has a mean lysis time of $\overline{\tau}$ of 12 minutes, the wild type has mean $\overline{\tau}$ 23 (i, iii, v) or 25 minutes (ii, iv, vi), and both have standard deviation $\Delta\tau = 0.01$ minutes.

By inspection of the population traces, we see that, within the stripe, the wild type delays fixation of the mutant (i) or reaches fixation itself (iii, v), by lysing later, infecting a large fraction of the available cells, and forcing the mutant to endure a significant delay between completing its final round of lysis and undergoing a passage, during which time is suffers virion loss due to super-adsorption and decay. If the mutant's mean lysis time is less than half that of the wild type (ii, iv, vi), this strategy is no longer viable, as the mutant's second round of lysis now secures almost all of the available resources.

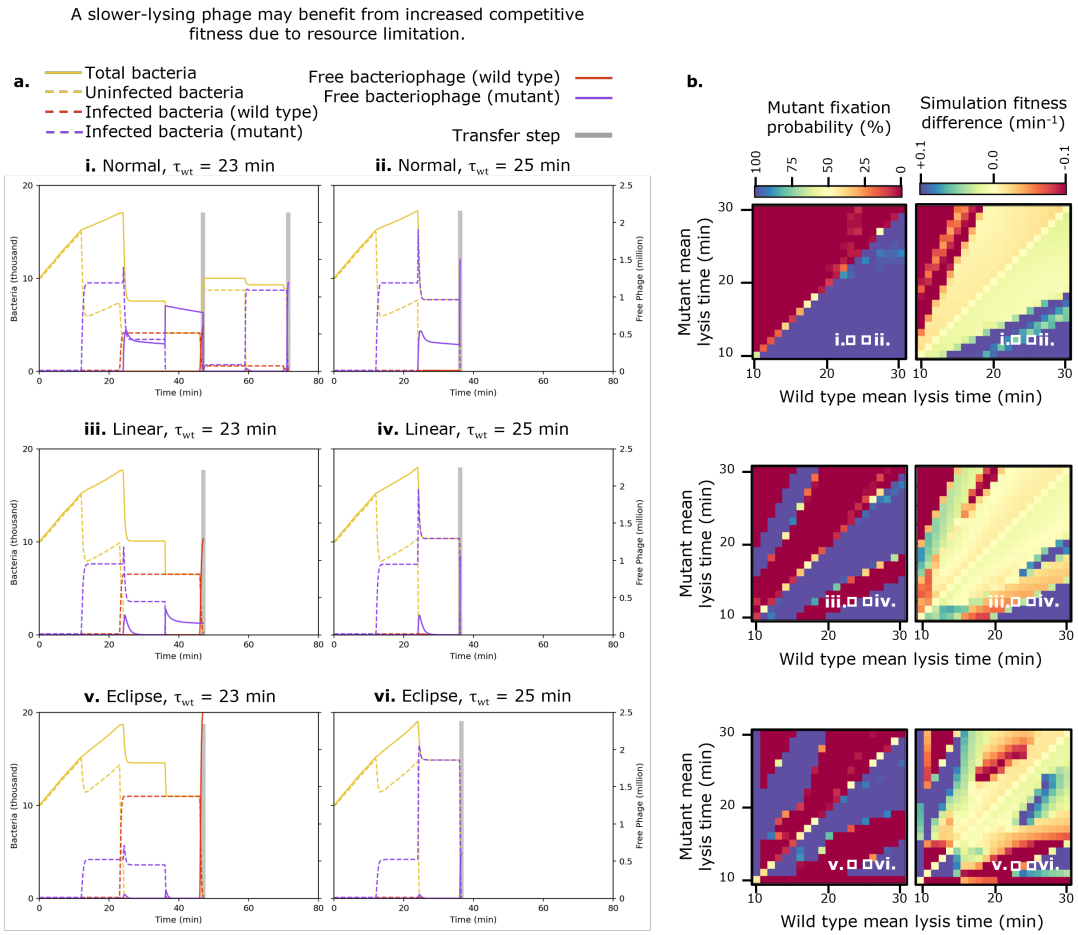

Fig. S7: **a.** Population vs time plots for all three burst size models to illustrate fitness "stripes". In all competitions, the mutant page had a mean lysis time of 12 minutes, and both phages had a lysis time std of 0.01 minutes. **b.** Copy of the data presented in Fig. 4: mutant fixation probability (left column) and fixation rate (right column) as a function of mutant and wild type mean lysis time. Parameter values corresponding to the traces on the left have been highlighted.

7.4.3 Population resonance requires super-adsorption and decay

To further demonstrate that the "stripes" on the serial passage fitness landscape arise from virion loss due to super adsorption and decay, we repeat all simulations discussed in section 3.2 (serial passage competition of two phage strains with different mean lysis times) under different conditions. In Fig S8a we reproduce the results of figure 4 without modification. In Fig S8b, we remove the possibility of virion loss by disabling both super-adsorption and decay ($A_{\max} = 1, \delta = 0$). Aside from the step fitness increase at $y = x/2$, agreement between the measured and predicted fitness differences is improved. When we further disable cell growth (Fig S8c) agreement improves further, though is still not complete.

A persistent distinction between predicted and measured fitness differences is that, in the serial passage case, because resources are finite, a number of step discontinuities in fitness will always be present, especially when lysis time std is small, since completing a lysis cycle even only slightly faster than an opponent is rewarded by a great share of resources.

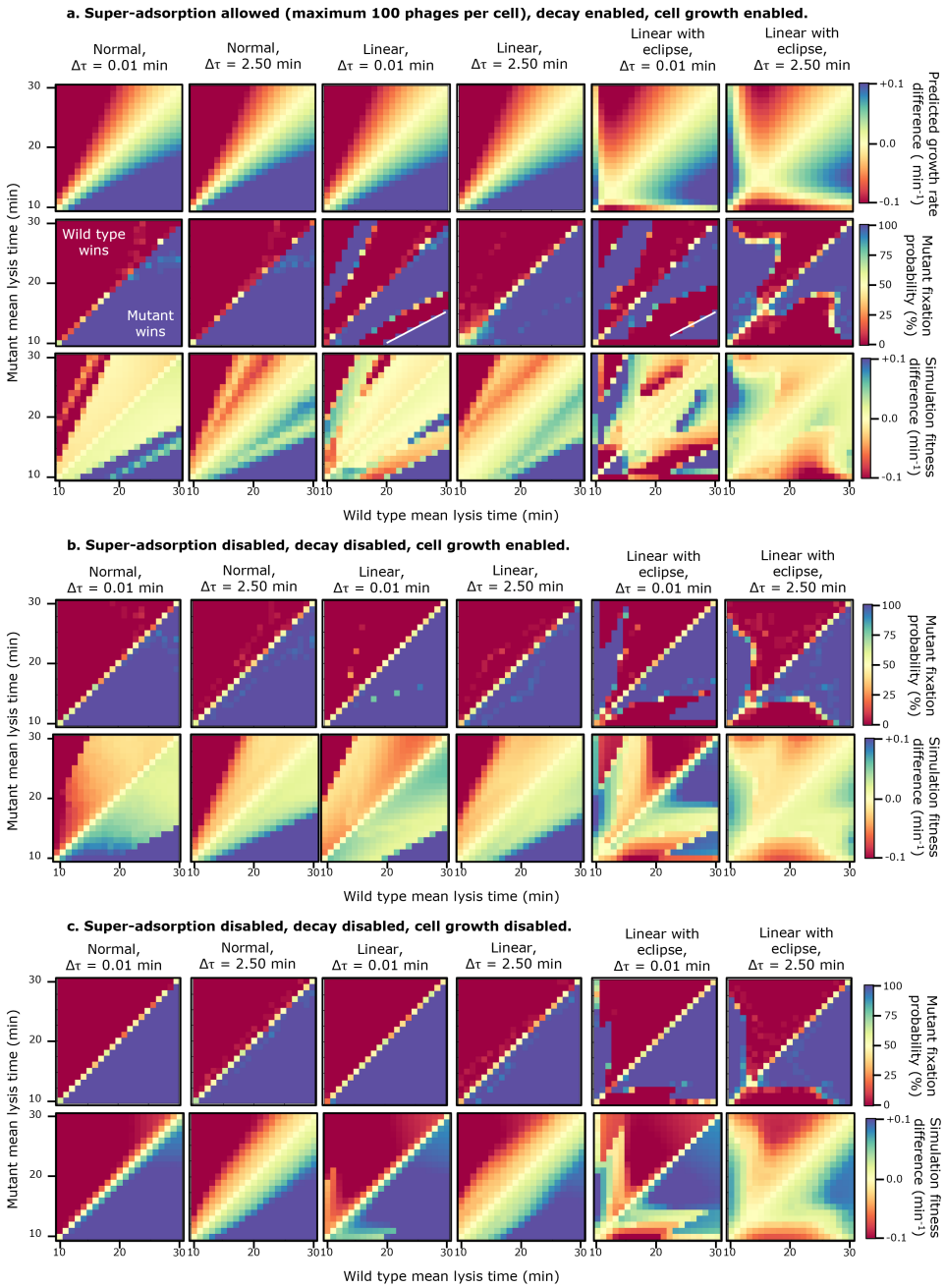

Fig. S8: Results of serial passage competition experiment, competing a wild type phage with one mean lysis time against a mutant with another. **a.** Same data is Fig 4, super-adsorption, free virion decay, and cell growth enabled ($A_{\max} = 100, \delta = 0.01, B_0 = 10,000, C = 100,000$). **b.** Super-adsorption and free virion decay disabled, cell growth enabled ($A_{\max} = 1, \delta = 0, B_0 = 10,000, C = 100,000$). **c.** Super-adsorption, free virion decay and cell growth disabled ($A_{\max} = 1, \delta = 0, B_0 = 10,000, C = 10,000$). Top row in a. is growth rate difference predicted by numerical integration, which assumes no super-adsorption or decay and abundant bacteria. Middle row in a. and top rows in b. and c. are mutant fixation probability. bottom rows in a. b. and c. are simulation fitness difference ΔF. In all rows apart from fixation probability the visual scale has been set to saturate at ± 0.1 min^{-1}.

7.4.4 Slower adsorption desynchronises lysis cycles, removing resonance stripes.

The adsorption rate α, initial bacterial number B_0 and simulated volume Vol used in the serial passage experiments discussed in section 3.2 and Fig 4 describe a system quite close to the high-adsorption limit ($\alpha B_0/Vol = 3$, giving a characteristic adsorption time of 20 seconds. To investigate the sensitivity of our results to this limit, we repeated the serial passage assay using the same parameters, except that the simulated volume Vol was increased by factor 100, representing a much sparser bacterial culture (Fig S9. This is mathematically equivalent to a reduction in adsorption rate.

In all three burst size models, numerically predicted growth rate predicts a global reduction in fitness difference $k_{\mathrm{mu}} - k_{\mathrm{wt}}$, across the whole of parameter space, since all phages will reproduce more slowly when the time to locate a host increases. The optimal lysis time predicted by the 'linear with eclipse' model also increases. As resources are harder to find, the explore-exploit trade-off shifts in favour of spending longer infecting each cell.

Simulated fitness difference ΔF and mutant fixation probability largely agree, with two interesting points to note. Firstly, the desynchronisation of lysis cycles caused by the adsorption delay removes any population resonance stripes. Second, the optimal lysis time for the 'linear with eclipse' model, shifts more than expected. Growth rate maximisation without considering adsorption time places the optimum at 15 minutes. Considering adsorption time places the optimum at about 17 minutes, and the simulation places the optimum at about 20 minutes. We interpret this as arising from resource limitation. Even though adsorption is now slow enough that super-adsorption is less of a concern, the limited nature of the available resources still rewards efficiency (taking longer to lyse but producing more offspring per cell).

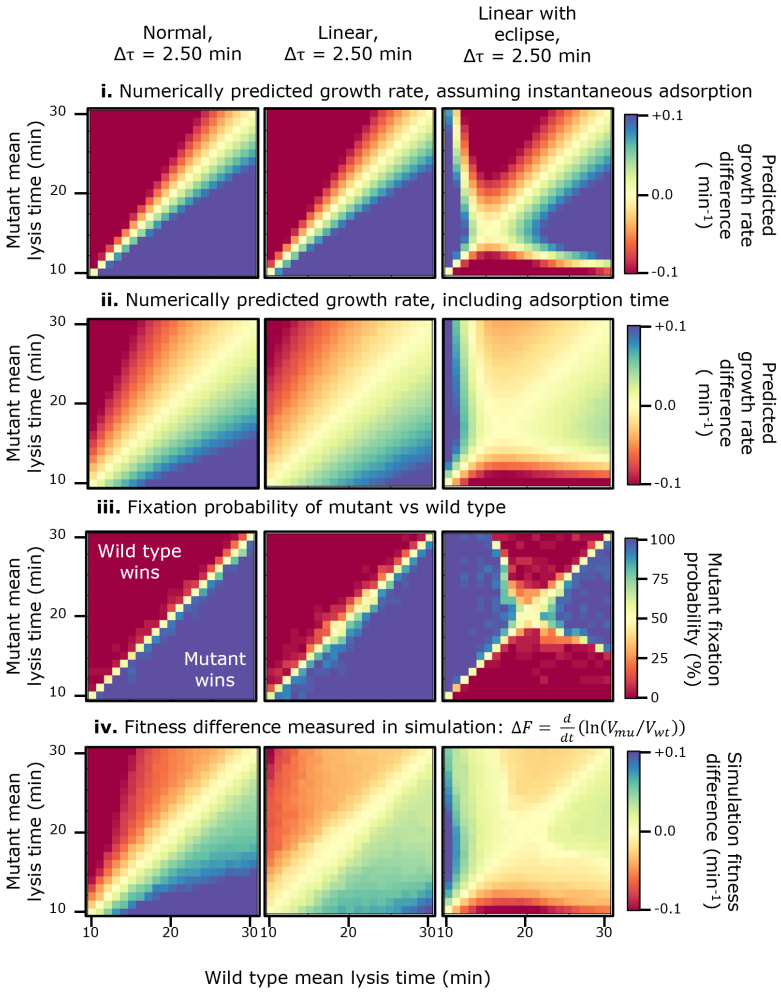

Fig. S9: Results of serial passage competition experiment, competing a wild type phage with one mean lysis time against a mutant with another, in a low-adsorption regime. **i.** Difference in numerically predicted growth rate, using equation 3 without correcting for adsorption time.**ii.** Difference in numerically predicted growth rate, using equation 3 convolved with an exponential distribution of mean $1/\alpha B_0$to correct for adsorption time. **iii.** Mutant fixation probability in stochastic simulation. **iv.** Fitness difference in stochastic simulation.

7.5 Mean-mean minimal simulation controls

7.5.1 Qualitative observations are robust to the choice of phage parameters

To confirm that our observations are not unique features of our specific parameter choices, we investigate a number of additional parameter choices using both numerical integration and a minimal "fast" simulation 7.5.3. First, we note that in our T7-*E. coli* inspired system, the range of lysis times available (10 to 30 minutes) is of similar order to the bacterial doubling time (20 minutes).

Changing the lysis time necessarily changes the burst size, so in order to investigate this relationship between lysis time and doubling time without confounding variables, we consider two phages in competition, predating bacteria with doubling times of 4, 9, 20 and 100 minutes (Fig S10).

We note that doubling times much greater than the lysis time do not introduce significantly and qualitatively new behaviour, but that doubling times much faster than lysis create a more complex fitness landscape. This is because, with bacteria doubling every 4 minutes (Fig S10vi), even a very small change in lysis time drastically alters the number of available cells. There is also an increase in the numerical instability of the 'fast' simulation as the bacterial doubling time decreases, visible as a yellow "speckle" across the fitness landscape.

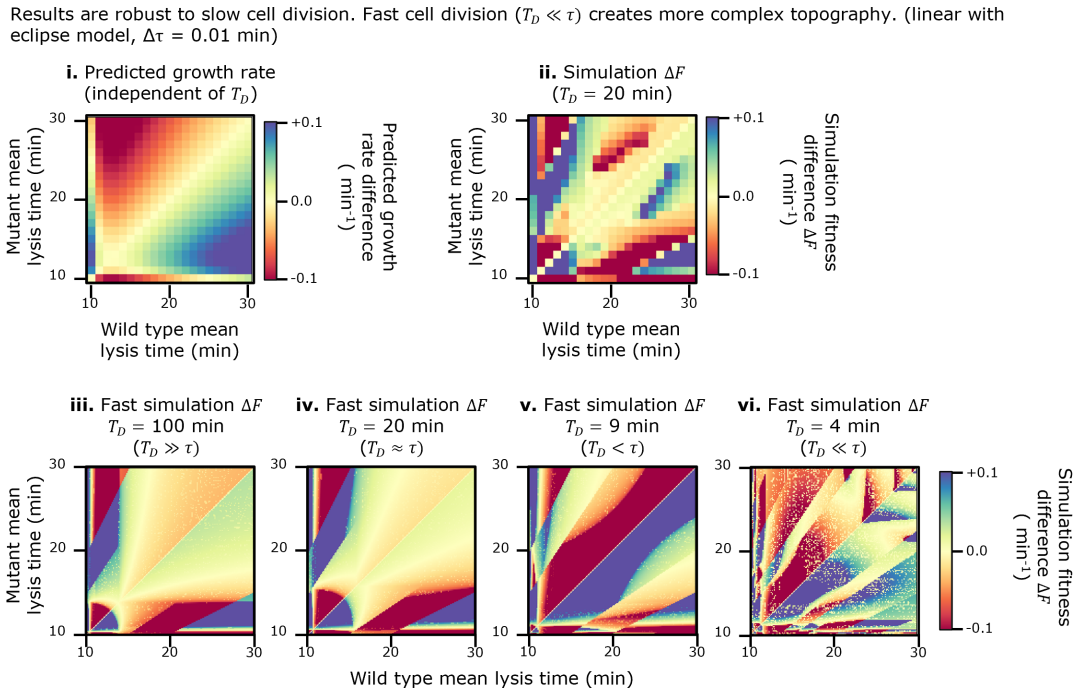

Fig. S10: **i.** Predicted growth rate difference between two phages in competition using the 'linear with eclipse' model, 0.01 min lysis time std. This prediction is made without reference to any bacterial doubling time, as it assumes bacteria are abundant. **ii.** Fitness difference of the same phages in serial passage simulation. Panels i and ii both appear in Fig 3.2, in rows i and iii respectively. **iii** to **vi**. Fast simulation results showing the effect of reducing bacterial doubling time. Panel iv corresponds to the same parameter values as panel ii, but using the 'fast' simulation 7.5.3 rather than the full simulation.

Next we note that burst sizes for different phage-bacteria pairs vary over several orders of magnitude [11]. To investigate the sensitivity of our results to our choice of burst sizes (centred on 150), we again consider two phages in competition, using the 'linear with eclipse' model, and vary either the maturation rate or eclipse period (Fig S11).

Numerical growth rate predictions (Fig S11a) suggest that varying m and ε alters the optimal lysis time, and the steepness of the iso-fitness contours, but does not introduce any new qualitative results. The 'fast' simulation suggests that very low maturation rates create a complex and unstable fitness topography, due to the

phage propagating very slowly, and thus the relative growth rate of the bacteria being very large.

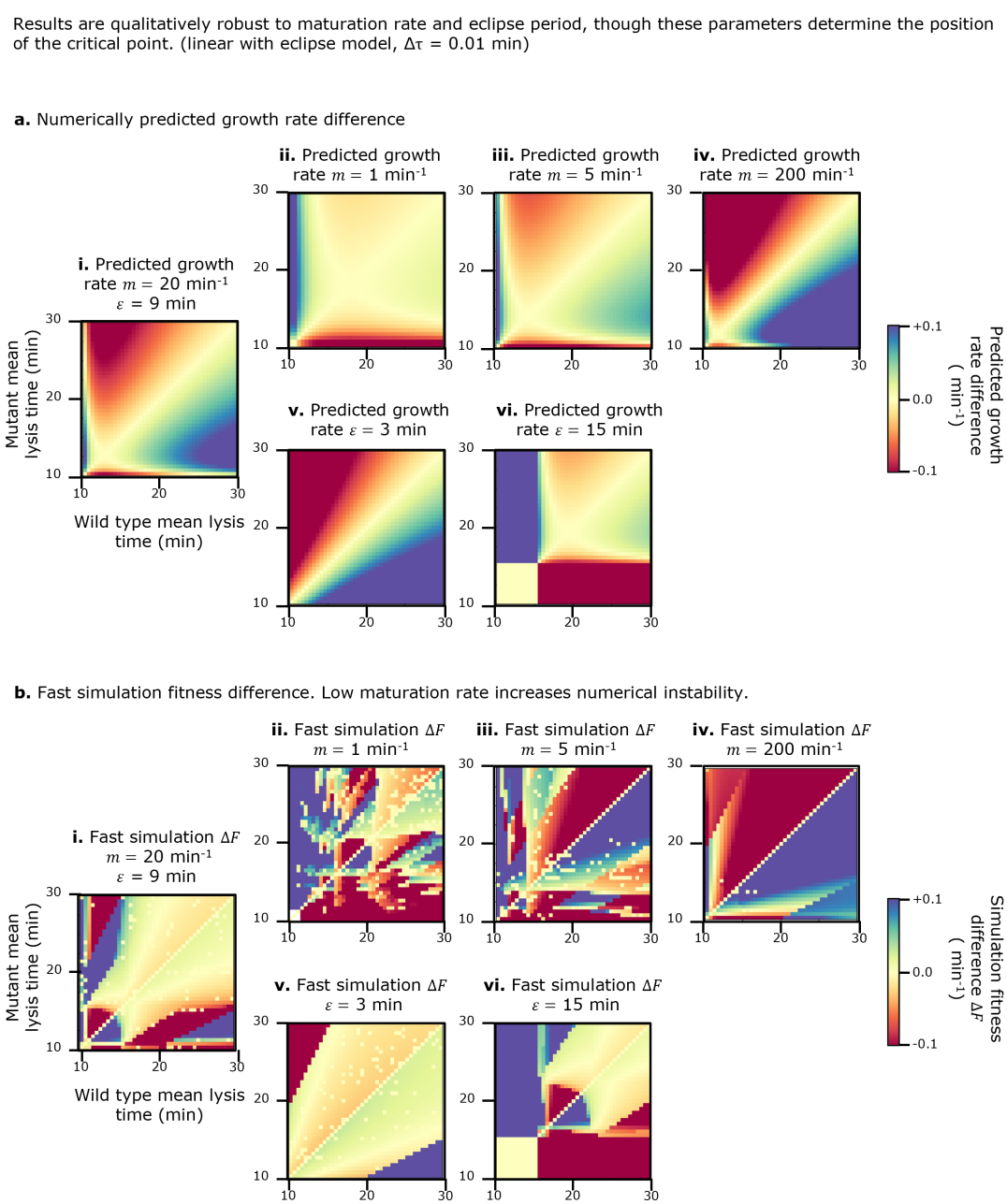

Fig. S11: **a.** Predicted growth rate difference between two phages in competition using the 'linear with eclipse' model, 0.01 min lysis time std, for the parameters used in the main paper (i), for varied maturation rates m (ii to iv) and varied eclipse periods ε (v to vi). **b.** Same as a. but showing 'fast' simulation fitness difference.

7.5.2 Population resonance depends on absolute cell count

To investigate the role of initial cell count in the population resonance phenomenon, we employ a fast-running "minimal" simulation. This simulation makes two additional assumptions: (i) that lysis times are totally deterministic, and (ii) that adsorption is instantaneous. This means all cells infected by a phage strain (mutant or wild type) will lyse at once, and the virions released will then immediately adsorb, up to the limit of maximum adsorbed virions per remaining cell. In figure S12, we plot the fitness difference ΔF between the mutant and wild type phage as their mean lysis times are varied from 1 to 50 minutes, for a range of initial cell numbers B_0. The 'normal' model was employed in this analysis, both phages using a common burst size of 150.

We note two distinct changes in the topography of the fitness landscape as the number of susceptible cells is increased, as well as a degree of numerical noise which is most prevalent when cell count is small (Fig S12i,ii). Since these plots are antisymmetric by construction, we will again limit discussion to the bottom right hand side of the parameter space, below the line $y = x$, without loss of generality.

First, we see a number of discontinuous changes in ΔF, each aligned with a particular ratio y/x (labelled explicitly in Fig S12xi). The most prominent of these is $y/x = 1/2$, which is visible to a greater or lesser extent in all panels. As the cell count is increased fitness discontinuities at $y/x = 1/3$, $y/x = 2/3$ and $y/x = 3/4$ appear. Starting at the line $y = x$, at which the mutant and wild type phages have the same lysis time, and moving downwards, each of these ratios represents the mutant gaining the ability to carry out an additional lysis cycle. For example, the step increase in fitness observed at $y/x = 1/2$ represents the mutant finishing its second lysis cycle and beginning a third, at the same time the wild type finished its first and begins its second. Larger cell counts allow for more rounds of lysis, thus more fitness discontinuities appear as the timing of the third, fourth and fifth rounds of lysis become relevant. There would be no advantage in the mutant ensuring its fourth round of lysis completed before the wild type's third round if there are insufficient cells to support that many rounds.

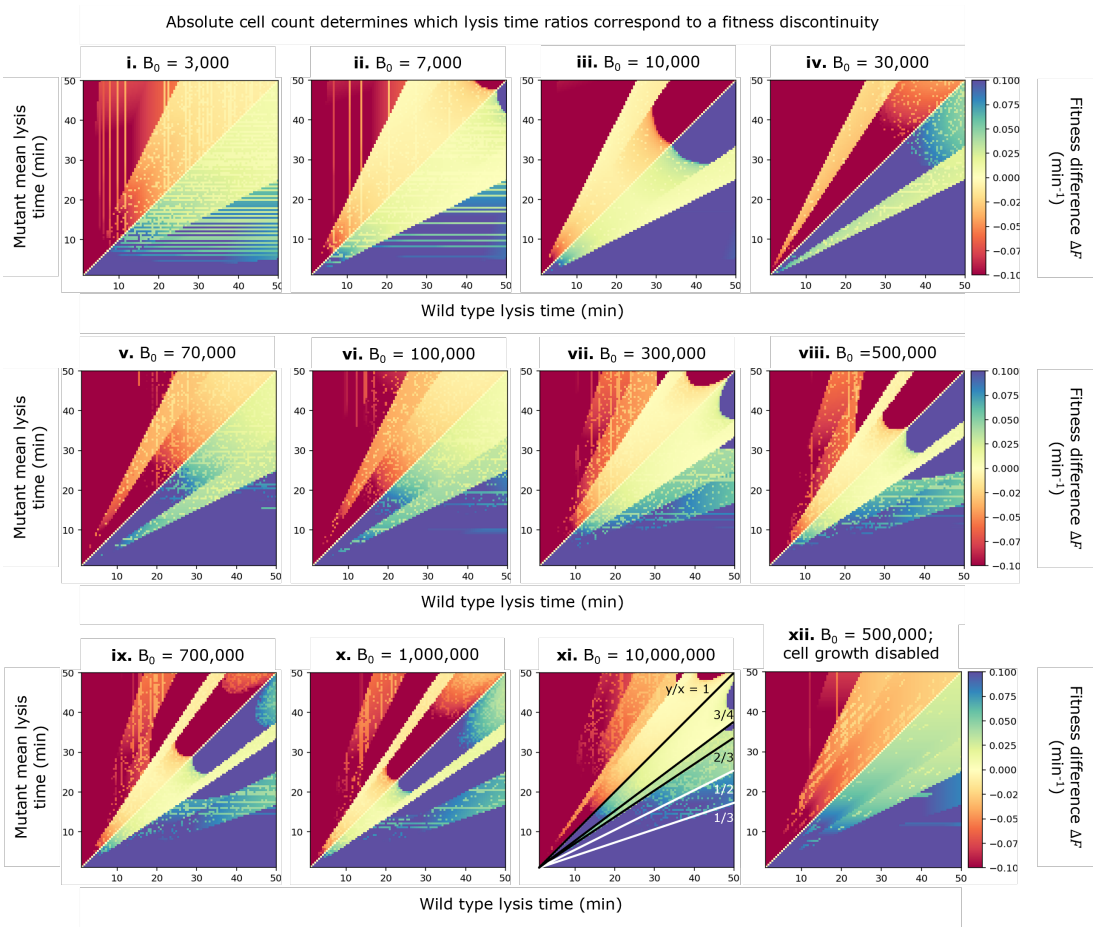

Fig. S12: Results of 'fast' simulation of a single serial passage cycle, competing a wild type phage with one mean lysis time against a mutant with another. The 'normal' model was used throughout, and intial cell count B_0 was varied for each panel. In all panels except xii cell growth was enabled with doubling time $T_D = 20$ minutes and no carrying capacity enforced. In panel xii, cell growth was disabled by setting $T_D = 20,000$ min.

Second, we see a screening of the fitness advantage obtained by a mutant which is only slightly faster than the wild type. In Fig S12i,ii,vi,vii,xi, a mutant phage with lysis time one minute faster than wild type displays only a slight competitive advantage. In Fig S12iii,iv,v,viii,ix,x, there is a region of parameter space for which such a mutant displays a significant fitness advantage (e.g. Fig S12iii, $B_0 = 10,000, \tau_{\text{wt}} = 40, \tau_{\text{mu}} = 39$). As cell count is increased, these regions seem to periodically appear at the top right corner of parameter space and move along the line $y = x$ towards the origin. These regions are first visible for initial bacteria counts B_0 of 7,000, 300,000 and 10,000,000, which are related by a common ratio of about 35. The significance of this value is not obvious, as it is much less than the bacteriophage's burst size of 150.

We compare Fig. S12viii and xii, which are both initialised with 500,000 cells. In viii cells grow with a doubling time of 20 minutes, whereas in xii cell growth is disabled. This has the effect that the fitness differences in the region just below $y = x$ have been homogenised - there is no longer a region of very minor fitness difference, and region of extreme fitness difference. We take this as evidence that this region arises due to the relationship between the number of phages inoculated at $t = 0$, and the number of cells available for lysis, which is a function of both how many cells are created at $t = 0$, and how many new cells are produced by division.

7.5.3 Implementation of fast minimal simulation

A number of control simulations were conducted using a faster, minimal simulation. This simulation makes two additional assumptions: that adsorption is instantaneous, and that lysis times and burst sizes are totally deterministic. This naturally means the minimal simulation cannot be used for investigation of lysis time distributions, but can be used to quickly measure the importance of properties such as maturation rate, eclipse period, adsorption limit, cell doubling time, and initial cell count. In the final two cases, the minimal simulation is particularly suitable as it is not object-based, so computational memory does not scale with the number of cells used, which may therefore be set arbitrarily high.

The simulation is based on eight variables, eight parameters, and three update rules, outlined in tables 6 to 9. The simulation variables are described in table 6.

Minimal simulation variables	
t	the time
B_T	the total number of bacteria
B_H	the number of healthy / uninfected bacteria
I_w	the number of bacteria infected by the wild type phage
I_m	the number of bacteria infected by the mutant phage
V_w	the number of free wild type phage
V_m	the number of free mutant phage
a	the total number of phages adsorbed to all living cells

Table 6: Variables used in fast minimal simulation

The simulation parameters are described in table 7.

Minimal simulation parameters	
B_0	initial bacteria count [-]
T_D	bacterial doubling time [min]
$A_{\max}$	maximum adsorbed virions per bacterium [-]
τ_w	wild type lysis time [min]
β_w	wild type burst size [-]
τ_m	mutant lysis time [min]
β_m	mutant burst size [-]
V_0	inital number of each virion type [-]

Table 7: Parameters used in fast minimal simulation

The update rules are 'adsorb', 'burst' and 'round off', implemented as follows.

Adsorb corresponds to as many virions as possible of one type (m or w) binding to bacteria. First, quantity P_0 is calculated, corresponding to the probability that a cell has no virions adsorb to it.

$$P_0 = \frac{e^{-V_w/B_T}}{B_T}$$

(i.e the $k = 0$ term of a Poisson distribution with mean V_w/B_T). Next, the number of virions that adsorb ΔV is taken as

$$\Delta V_i = \max(B_T \cdot A_{\max} - a, V_i).$$

That is, virions adsorb until either there are no free virions remaining, or the available bacteria are saturated.

The variables are updated as described in table 8.

'Adsorb' update rule	
$t \to t$	this step is assumed to be instantaneous, so the 'time' variable is not updated.
$B_T \to B_T$	the total number of bacteria does not change.
$B_H \to B_H \cdot P_0$	fraction P_0 of bacteria are not adsorbed to.
$I_i \to I_i + B_H(1-P_0)$	healthy cells have probability $(1-P_0)$ to become infected by the appropriate phage $i \in \{w, m\}$.
$V_i \to V_i - \Delta V_i$	the number of free phage is reduced by the number that were able to adsorb.
$a \to a + \Delta V$	the total adsorbed phages is updated to include those just adsorbed

Table 8: 'Adsorption' step variable update rules

Burst corresponds to an interval of time Δt passing, followed by all cells infected by one phage type (m or w) lysing simultaneously, releasing their progeny. First, cell growth factor G is calculated as

$$G = e^{\frac{\ln(2)\cdot\Delta t}{T_D}}.$$

The variables are then updated as described in table 9.

'Burst' update rule	
$t \to t + \Delta t$	t is advanced by the time interval.
$B_T \to B_T - I_i + B_H \cdot G$	the total number of bacteria is reduced by infected cells lysing, but increased by healthy cells dividing.
$B_H \to B_H \cdot G$	the number of healthy cells is increased by the growth factor.
$I_i \to 0$	all cells infected by the appropriate phage are lysed $i \in \{w, m\}$.
$V_i \to V_i + I_i \cdot \beta_i$	the number of free phage is increased by the number of lysing cells multiplied by the burst size
$a \to a \cdot (1 - \frac{I_i}{I_i + I_j})$	the total count of phages adsorbed to living cells is reduced by the fraction of infected cells which just lysed. $i \in \{w, m\}$, $j \in \{w, m\}$, $j \neq i$.

Table 9: 'Burst' step variable update rules

Round off simply rounds all variables other than t to the nearest integer.

The simulation begins with an an **adsorb** update called for both phage species. After that, the simulation enters a loop of checking when the next lysis event should be (which is the next smallest integer multiple of either τ_w or τ_m), jumping forwards in time to that event ($\Delta t = t_{\text{nextlysis}} - t$), then calling the **burst, adsorb** and **round off** update rules. This process continues until either (a) all cells are dead, or (b) there are no infected cells or free phage remaining, which can happen if both burst sizes are 0.

The fitness difference ΔF is then determined through

$$\Delta F = \frac{\ln\left(\frac{V_m}{V_w}\right)}{t}$$

for final values of V_m, V_w, and t.

In order that the simulation can always uniquely determine which lysis event should happen next, the lysis times for the mutant phage are all increased by 2^{-10} minutes.

Given the simplicity of this simulation, we see remarkable qualitative agreement to the full stochastic simulation, including correct prediction of the existence and position of "stripes" (compare Fig 4biii leftmost column to Fig S12iii).

7.6 Assay comparison reveals weaker selective pressure in plaque assay and broadening of resonance stripes at high lysis time std

To aid comparison between the serial passage (Fig 5) and plaque expansion (Fig 6), we directly subtract the fitness advantage displayed by the mutant in one assay from another (Fig S13).

Note in particular the large blue region in the first row under the 'linear with eclipse' model, and corresponding brown region in the third row. These represent the mutant achieving fixation by population resonance in the serial passage experiment (i) but not in the plaque expansion (iii).

We use a new colour-map for this plot, as blue and brown correspond to the mutant displaying a larger fitness in one assay versus another, not displaying a fitness advantage over the wild type.

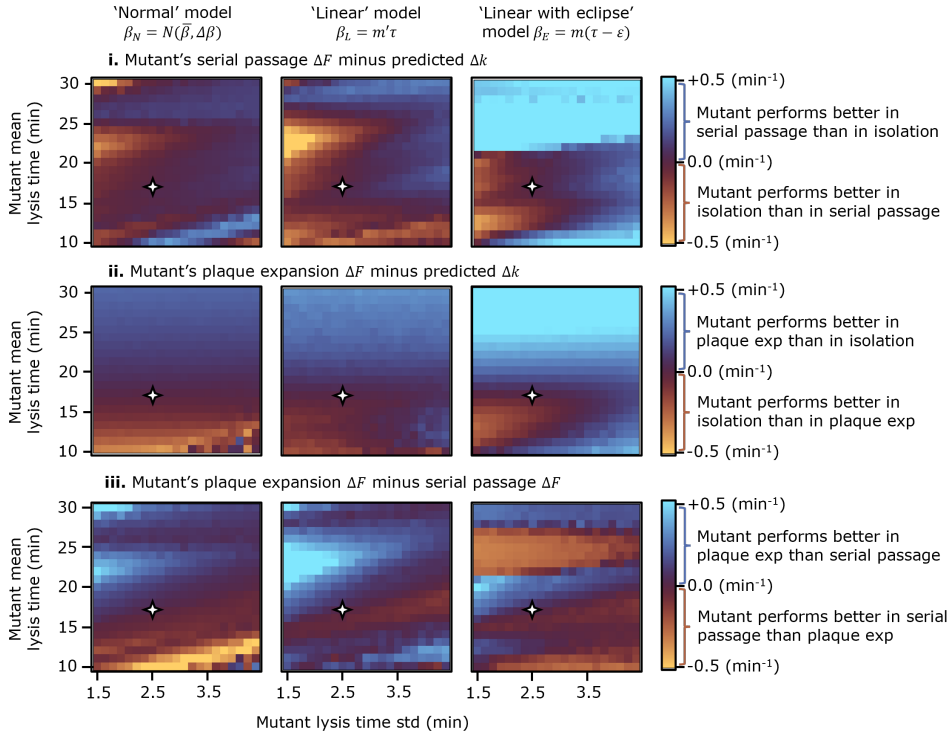

Fig. S13: Assay comparison for serial passage competition experiment, competing a wild type phage with lysis time mean 17 min, std 2.5 min against a mutant with varied lysis time mean (y axis) and std (x axis). **i.** Difference between mutant's fitness advantage in serial passage vs predicted advantage based on growth rate in isolation $\Delta F_{\mathrm{SP}} - (k_{\mathrm{mu}} - k_{\mathrm{wt}})$. **ii.** Difference between mutant's fitness advantage in plaque expansion vs predicted advantage based on growth rate in isolation $\Delta F_{\mathrm{PE}} - (k_{\mathrm{mu}} - k_{\mathrm{wt}})$. **iii.** Difference between mutant's fitness advantage in serial passage vs fitness advantage in serial passage $\Delta F_{\mathrm{PE}} - \Delta F_{\mathrm{SP}}$. Axes are scaled such that each pixel step in the y direction corresponds to a 1 minute change in mean lysis time, while each pixel step in the x direction corresponds to an equivalent fractional change in lysis time std versus the wild type value: 2.5/17 minutes. The four-point star on all panels labels the point in parameter space at which both phages have exactly the same parameters.

7.7 The secondary fitness maximum observed under the 'linear with eclipse' model is explained by population resonance

To demonstrate that population resonance is responsible for the high fitness region towards the top of the 'linear with eclipse' fitness map in Fig 5ii, we repeat the simulation using either different initial cell counts (Fig S14 i to v), or under 'conservative' conditions (no super-adsorption or decay, Fig S14vi).

As the cell count is increased from 3,000 to 70,000, the high fitness region appears and disappears again, hence the name "resonance", while the high fitness region towards the bottom of the plot remains largely conserved.

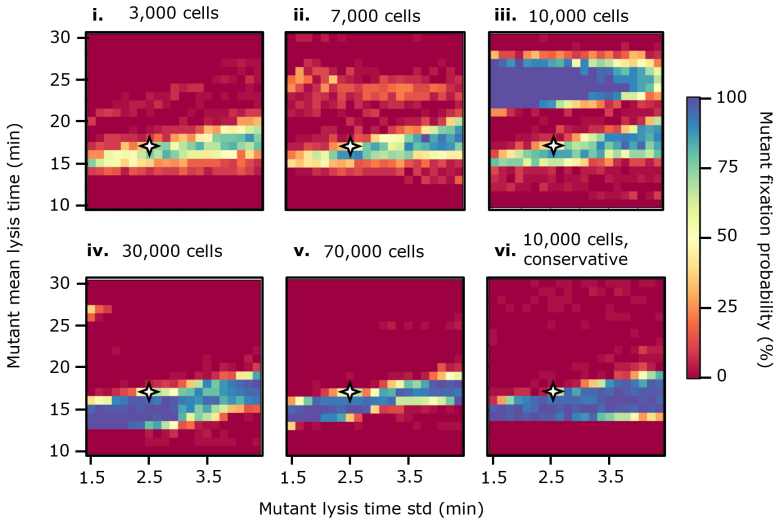

Fig. S14: Mutant fixation probability in serial passage competition experiment, competing a wild type phage with lysis time mean 17 min, std 2.5 min against a mutant with varied lysis time mean (y axis) and std (x axis). Super-adsorption and decay are permitted in panels i to v, but disabled in panel vi. The initial number of cells B_0 used in each simulation can be seen above each panel. Panel iii corresponds to the set up used in the main paper.

References

[1] Anne Chevallereau et al. "Interactions between bacterial and phage communities in natural environments". In: *Nature Reviews Microbiology* 20.1 (Jan. 2022). Publisher: Nature Publishing Group, pp. 49–62. ISSN: 1740-1534. DOI: 10.1038/s41579-021-00602-y. URL: https://www.nature.com/articles/s41579-021-00602-y (visited on 01/22/2025).

[2] Charles Schmidt. "Phage therapy's latest makeover". In: *Nature Biotechnology* 37.6 (June 1, 2019). Bandiera_abtest: a Cg_type: Nature Research Journals Number: 6 Primary_atype: News Publisher: Nature Publishing Group, pp. 581–586. ISSN: 1546-1696. DOI: 10.1038/s41587-019-0133-z. URL: https://www.nature.com/articles/s41587-019-0133-z (visited on 01/25/2022).

[3] Review on Antimicrobial Resistance. *Tackling Drug-Resistant Infections Globally: Final Report and Recommendations*. UK Government and Wellcome Trust, 2016, p. 80. URL: https://amr-review.org/sites/default/files/160525_Final%20paper_with%20cover.pdf (visited on 01/30/2022).

[4] William C. Summers. "The strange history of phage therapy". In: *Bacteriophage* 2.2 (Apr. 1, 2012). Publisher: Taylor & Francis _eprint: https://doi.org/10.4161/bact.20757, pp. 130–133. ISSN: null. DOI: 10.4161/bact.20757. URL: https://doi.org/10.4161/bact.20757 (visited on 06/30/2025).

[5] Félix d'Herelle. "An Invisible Microbe that is Antagonistic to the Dysentery Bacillus (Sur un microbe invisible antagonsite des bacilles dysenteriques." In: *Comptes rendus Acad. Sciences* 165 (1917), pp. 373–375.

[6] Rui Zhu et al. "In Vitro and In Vivo Antibacterial Efficacy of Bacteriophage Combined with Tigecycline Against Carbapenem-Resistant Klebsiella pneumoniae and Characterization of Phage Resistant Mutants". In: *Frontiers in Cellular and Infection Microbiology* 15 (June 26, 2025). Publisher: Frontiers. ISSN: 2235-2988. DOI: 10.3389/fcimb.2025.1610625. URL: https://www.frontiersin.org/journals/cellular-and-infection-microbiology/articles/10.3389/fcimb.2025.1610625/full (visited on 06/30/2025).

[7] A. Vieira et al. "Phage therapy to control multidrug-resistant Pseudomonas aeruginosa skin infections: in vitro and ex vivo experiments". In: *European Journal of Clinical Microbiology & Infectious Diseases* 31.11 (Nov. 1, 2012), pp. 3241–3249. ISSN: 1435-4373. DOI: 10.1007/s10096-012-1691-x. URL: https://doi.org/10.1007/s10096-012-1691-x (visited on 06/30/2025).

[8] M. Delbrück. "ADSORPTION OF BACTERIOPHAGE UNDER VARIOUS PHYSIOLOGICAL CONDITIONS OF THE HOST". In: *The Journal of General Physiology* 23.5 (May 20, 1940), pp. 631–642. ISSN: 0022-1295. URL: https://www.ncbi.nlm.nih.gov/pmc/articles/PMC2237952/ (visited on 04/17/2023).

[9] E. L. Ellis and M. Delbrück. "THE GROWTH OF BACTERIOPHAGE". In: *The Journal of General Physiology* 22.3 (Jan. 20, 1939), pp. 365–384. ISSN: 0022-1295. DOI: 10.1085/jgp.22.3.365.

[10] Albert P. Krueger. "THE SORPTION OF BACTERIOPHAGE BY LIVING AND DEAD SUSCEPTIBLE BACTERIA". In: *The Journal of General Physiology* 14.4 (Mar. 20, 1931), pp. 493–516. ISSN: 0022-1295. URL: https://www.ncbi.nlm.nih.gov/pmc/articles/PMC2141123/ (visited on 05/27/2023).

[11] Marian Dominguez-Mirazo et al. "Accounting for cellular-level variation in lysis: implications for virus–host dynamics". In: *mBio* 0.0 (July 19, 2024). Publisher: American Society for Microbiology, e01376–24. DOI: 10.1128/mbio.01376-24. URL: https://journals.asm.org/doi/10.1128/mbio.01376-24 (visited on 08/01/2024).

[12] Sherin Kannoly et al. "Single-Cell Approach Reveals Intercellular Heterogeneity in Phage-Producing Capacities". In: *Microbiology Spectrum* 11.1 (Dec. 21, 2022). Publisher: American Society for Microbiology, e02663–21. DOI: 10.1128/spectrum.02663-21. URL: https://journals.asm.org/doi/full/10.1128/spectrum.02663-21 (visited on 06/30/2025).

[13] Sílvio B. Santos et al. "Population Dynamics of a Salmonella Lytic Phage and Its Host: Implications of the Host Bacterial Growth Rate in Modelling". In: *PLOS ONE* 9.7 (July 22, 2014). Publisher: Public Library of Science, e102507. ISSN: 1932-6203. DOI: 10.1371/journal.pone.0102507. URL: https://journals.plos.org/plosone/article?id=10.1371/journal.pone.0102507 (visited on 06/30/2025).

[14] Sherin Kannoly, Abhyudai Singh, and John J. Dennehy. "An Optimal Lysis Time Maximizes Bacteriophage Fitness in Quasi-Continuous Culture". In: *mBio* 13.3 (Apr. 25, 2022). Publisher: American Society for Microbiology, e03593–21. DOI: 10.1128/mbio.03593-21. URL: https://journals.asm.org/doi/full/10.1128/mbio.03593-21 (visited on 06/30/2025).

[15] Shazeeda Koonjan, Carlos Cardoso Palacios, and Anders S. Nilsson. "Population Dynamics of a Two Phages–One Host Infection System Using Escherichia coli Strain ECOR57 and Phages vB_EcoP_SU10 and vB_EcoD_SU57". In: *Pharmaceuticals* 15.3 (Mar. 2022). Number: 3 Publisher: Multidisciplinary Digital Publishing Institute, p. 268. ISSN: 1424-8247. DOI: 10.3390/ph15030268. URL: https://www.mdpi.com/1424-8247/15/3/268 (visited on 04/27/2023).

[16] Katja Šivec and Aleš Podgornik. "Determination of bacteriophage growth parameters under cultivating conditions". In: *Applied Microbiology and Biotechnology* 104.20 (Oct. 2020), pp. 8949–8960. ISSN: 1432-0614. DOI: 10.1007/s00253-020-10866-8.

[17] Romain Gallet, Yongping Shao, and Ing-Nang Wang. "High adsorption rate is detrimental to bacteriophage fitness in a biofilm-like environment". In: *BMC Evolutionary Biology* 9.1 (Oct. 5, 2009), p. 241. ISSN: 1471-2148. DOI: 10.1186/1471-2148-9-241. URL: https://doi.org/10.1186/1471-2148-9-241 (visited on 05/12/2023).

[18] Daniel Campos, Vicenç Méndez, and Sergei Fedotov. "The effects of distributed life cycles on the dynamics of viral infections". In: *Journal of Theoretical Biology* 254.2 (Sept. 21, 2008), pp. 430–438. ISSN: 0022-5193. DOI: 10.1016/j.jtbi.2008.05.035. URL: https://www.sciencedirect.com/science/article/pii/S0022519308002932 (visited on 06/19/2023).

[19] Richard H. Heineman and James J. Bull. "Testing optimality with experimental evolution: lysis time in a bacteriophage". In: *Evolution; International Journal of Organic Evolution* 61.7 (July 2007), pp. 1695–1709. ISSN: 0014-3820. DOI: 10.1111/j.1558-5646.2007.00132.x.

[20] Dongwoo Chae. "Phage-host-immune system dynamics in bacteriophage therapy: basic principles and mathematical models". In: *Translational and Clinical Pharmacology* 31.4 (Dec. 2023), pp. 167–190. ISSN: 2289-0882. DOI: 10.12793/tcp.2023.31.e17. URL: https://www.ncbi.nlm.nih.gov/pmc/articles/PMC10772058/ (visited on 06/30/2025).

[21] Anders S. Nilsson. "Cocktail, a Computer Program for Modelling Bacteriophage Infection Kinetics". In: *Viruses* 14.11 (Nov. 2022). Number: 11 Publisher: Multidisciplinary Digital Publishing Institute, p. 2483. ISSN: 1999-4915. DOI: 10.3390/v14112483. URL: https://www.mdpi.com/1999-4915/14/11/2483 (visited on 06/30/2025).

[22] Quentin J. Leclerc, Jodi A. Lindsay, and Gwenan M. Knight. "Modelling the synergistic effect of bacteriophage and antibiotics on bacteria: Killers and drivers of resistance evolution". In: *PLOS Computational Biology* 18.11 (Nov. 30, 2022). Publisher: Public Library of Science, e1010746. ISSN: 1553-7358. DOI: 10.1371/journal.pcbi.1010746. URL: https://journals.plos.org/ploscompbiol/article?id=10.1371/journal.pcbi.1010746 (visited on 06/30/2025).

[23] Ing-Nang Wang. "Lysis Timing and Bacteriophage Fitness". In: *Genetics* 172.1 (Jan. 1, 2006), pp. 17–26. ISSN: 1943-2631. DOI: 10.1534/genetics.105.045922. URL: https://doi.org/10.1534/genetics.105.045922 (visited on 05/12/2023).

[24] Joaquim Fort and Vicenç Méndez. "Time-Delayed Spread of Viruses in Growing Plaques". In: *Physical Review Letters* 89.17 (Oct. 8, 2002). Publisher: American Physical Society, p. 178101. DOI: 10.1103/PhysRevLett.89.178101. URL: https://link.aps.org/doi/10.1103/PhysRevLett.89.178101 (visited on 07/04/2025).

[25] J Yin and J S McCaskill. "Replication of viruses in a growing plaque: a reaction-diffusion model." In: *Biophysical Journal* 61.6 (June 1992), pp. 1540–1549. ISSN: 0006-3495. URL: https://www.ncbi.nlm.nih.gov/pmc/articles/PMC1260448/ (visited on 03/06/2024).

[26] Jacopo Marchi et al. *Stable coexistence and transport of lytic phage infections with migrating bacterial hosts*. Pages: 2025.04.18.649568 Section: New Results. Apr. 21, 2025. DOI: 10.1101/2025.04.18.649568. URL: https://www.biorxiv.org/content/10.1101/2025.04.18.649568v2 (visited on 05/22/2025).

[27] Melinda Choua et al. "The effect of viral plasticity on the persistence of host-virus systems". In: *Journal of Theoretical Biology* 498 (Aug. 7, 2020), p. 110263. ISSN: 0022-5193. DOI: 10.1016/j.jtbi.2020.110263. URL: https://www.sciencedirect.com/science/article/pii/S0022519320301181 (visited on 10/05/2022).

[28] Gabor Beke, Matej Stano, and Lubos Klucar. "Modelling the interaction between bacteriophages and their bacterial hosts". In: *Mathematical Biosciences* 279 (Sept. 1, 2016), pp. 27–32. ISSN: 0025-5564. DOI: 10.1016/j.mbs.2016.06.009. URL: https://www.sciencedirect.com/science/article/pii/S0025556416300700 (visited on 06/30/2025).

[29] Michael B. Elowitz et al. “Stochastic Gene Expression in a Single Cell”. In: *Science* 297.5584 (Aug. 16, 2002). Publisher: American Association for the Advancement of Science, pp. 1183–1186. DOI: 10.1126/science.1070919. URL: https://www.science.org/doi/10.1126/science.1070919 (visited on 07/11/2025).

[30] Michael Hunter and Diana Fusco. “Superinfection exclusion: A viral strategy with short-term benefits and long-term drawbacks”. In: *PLOS Computational Biology* 18.5 (May 10, 2022). Publisher: Public Library of Science, e1010125. ISSN: 1553-7358. DOI: 10.1371/journal.pcbi.1010125. URL: https://journals.plos.org/ploscompbiol/article?id=10.1371/journal.pcbi.1010125 (visited on 05/29/2023).

[31] Andrés Valdez et al. “Biomechanical modeling of spatiotemporal bacteria-phage competition”. In: *Communications Physics* 8.1 (Apr. 8, 2025). Publisher: Nature Publishing Group, p. 139. ISSN: 2399-3650. DOI: 10.1038/s42005-025-02078-1. URL: https://www.nature.com/articles/s42005-025-02078-1 (visited on 07/04/2025).

[32] Blessing Emerenini et al. “The effect of environmental factors in biofilm and phage interactions in Agent Based Model”. In: *arXiv* (Feb. 22, 2025). URL: https://doi.org/10.48550/arXiv.2502.18507 (visited on 06/30/2025).

[33] Michael Hunter et al. “Virus-Host Interactions Shape Viral Dispersal Giving Rise to Distinct Classes of Traveling Waves in Spatial Expansions”. In: *Physical Review X* 11.2 (June 29, 2021). Publisher: American Physical Society, p. 021066. DOI: 10.1103/PhysRevX.11.021066. URL: https://link.aps.org/doi/10.1103/PhysRevX.11.021066 (visited on 06/21/2023).

[34] Alison Cameron et al. *Keep Your Frenemies Closer: Bacteriophage That Benefit Their Hosts Evolve to be More Temperate*. 2022. URL: https://ecoevorxiv.org/repository/object/3802/download/7521/.

[35] Abhyudai Singh and John J. Dennehy. “Stochastic holin expression can account for lysis time variation in the bacteriophage ”. In: *Journal of The Royal Society Interface* 11.95 (June 6, 2014). Publisher: Royal Society, p. 20140140. DOI: 10.1098/rsif.2014.0140. URL: https://royalsocietypublishing.org/doi/10.1098/rsif.2014.0140 (visited on 07/04/2025).

[36] John J. Dennehy and Ing-Nang Wang. “Factors influencing lysis time stochasticity in bacteriophage lambda”. In: *BMC Microbiology* 11.1 (Aug. 2, 2011), p. 174. ISSN: 1471-2180. DOI: 10.1186/1471-2180-11-174. URL: https://doi.org/10.1186/1471-2180-11-174 (visited on 10/05/2022).

[37] Charlie Wedd et al. *Single-cell imaging of the lytic phage life cycle in bacteria*. Pages: 2024.04.11.588870 Section: New Results. Oct. 22, 2024. DOI: 10.1101/2024.04.11.588870. URL: https://www.biorxiv.org/content/10.1101/2024.04.11.588870v3 (visited on 06/30/2025).

[38] Antrea Pavlou et al. “Single-cell data reveal heterogeneity of investment in ribosomes across a bacterial population”. In: *Nature Communications* 16.1 (Jan. 2, 2025). Publisher: Nature Publishing Group, p. 285. ISSN: 2041-1723. DOI: 10.1038/s41467-024-55394-5. URL: https://www.nature.com/articles/s41467-024-55394-5 (visited on 07/04/2025).

[39] Kimberly M. Davis and Ralph R. Isberg. “Defining heterogeneity within bacterial populations via single cell approaches”. In: *BioEssays* 38.8 (2016). _eprint: https://onlinelibrary.wiley.com/doi/pdf/10.1002/bies.201500121, pp. 782–790. ISSN: 1521-1878. DOI: 10.1002/bies.201500121. URL: https://onlinelibrary.wiley.com/doi/abs/10.1002/bies.201500121 (visited on 07/14/2025).

[40] Lingchong You, Patrick F. Suthers, and John Yin. “Effects of Escherichia coli Physiology on Growth of Phage T7 In Vivo and In Silico”. In: *Journal of Bacteriology* 184.7 (Apr. 2002), pp. 1888–1894. ISSN: 0021-9193. DOI: 10.1128/JB.184.7.1888-1894.2002. URL: https://www.ncbi.nlm.nih.gov/pmc/articles/PMC134924/ (visited on 05/05/2023).

[41] Erin L. Attrill et al. “Individual bacteria in structured environments rely on phenotypic resistance to phage”. In: *PLOS Biology* 19.10 (Oct. 12, 2021). Publisher: Public Library of Science, e3001406. ISSN: 1545-7885. DOI: 10.1371/journal.pbio.3001406. URL: https://journals.plos.org/plosbiology/article?id=10.1371/journal.pbio.3001406 (visited on 05/15/2023).

[42] Maxime Schwartz. “The adsorption of coliphage lambda to its host: Effect of variations in the surface density of receptor and in phage-receptor affinity”. In: *Journal of Molecular Biology* 103.3 (May 25, 1976), pp. 521–536. ISSN: 0022-2836. DOI: 10.1016/0022-2836(76)90215-1. URL: https://www.sciencedirect.com/science/article/pii/0022283676902151 (visited on 07/14/2025).

[43] Stephen Tobias Abedon. “Bacteriophage Adsorption: Likelihood of Virion Encounter with Bacteria and Other Factors Affecting Rates”. In: *Antibiotics* 12.4 (Apr. 2023). Number: 4 Publisher: Multidisciplinary Digital Publishing Institute, p. 723. ISSN: 2079-6382. DOI: 10.3390/antibiotics12040723. URL: https://www.mdpi.com/2079-6382/12/4/723 (visited on 07/04/2025).

[44] James J. Bull, Richard H. Heineman, and Claus O. Wilke. “The Phenotype-Fitness Map in Experimental Evolution of Phages”. In: *PLOS ONE* 6.11 (Nov. 22, 2011). Publisher: Public Library of Science, e27796. ISSN: 1932-6203. DOI: 10.1371/journal.pone.0027796. URL: https://journals.plos.org/plosone/article?id=10.1371/journal.pone.0027796 (visited on 07/04/2025).

[45] Mikihiro Hashimoto et al. “Noise-driven growth rate gain in clonal cellular populations”. In: *Proceedings of the National Academy of Sciences* 113.12 (Mar. 22, 2016). Publisher: Proceedings of the National Academy of Sciences, pp. 3251–3256. DOI: 10.1073/pnas.1519412113. URL: https://www.pnas.org/doi/10.1073/pnas.1519412113 (visited on 05/09/2023).

[46] E. O. Powell. “Growth Rate and Generation Time of Bacteria, with Special Reference to Continuous Culture”. In: *Microbiology* 15.3 (1956). Publisher: Microbiology Society, pp. 492–511. ISSN: 1465-2080. DOI: 10.1099/00221287-15-3-492. URL: https://www.microbiologyresearch.org/content/journal/micro/10.1099/00221287-15-3-492 (visited on 05/11/2023).

[47] Bálint Kiss et al. “Imaging the Infection Cycle of T7 at the Single Virion Level”. In: *International Journal of Molecular Sciences* 23.19 (Jan. 2022). Number: 19 Publisher: Multidisciplinary Digital Publishing Institute, p. 11252. ISSN: 1422-0067. DOI: 10.3390/ijms231911252. URL: https://www.mdpi.com/1422-0067/23/19/11252 (visited on 01/10/2023).

[48] Gunther Stent. *Molecular Biology of Bacterial Viruses*. A Series of Books in Biology 17. United States of America: W. H. Freeman and Company, 1963. 474 pp.

[49] Yongping Shao and Ing-Nang Wang. “Bacteriophage Adsorption Rate and Optimal Lysis Time”. In: *Genetics* 180.1 (Sept. 1, 2008), pp. 471–482. ISSN: 1943-2631. DOI: 10.1534/genetics.108.090100. URL: https://doi.org/10.1534/genetics.108.090100 (visited on 09/15/2023).

[50] Hai Xu et al. “Biological Characterization and Evolution of Bacteriophage T7-holin During the Serial Passage Process”. In: *Frontiers in Microbiology* 12 (2021), p. 705310. ISSN: 1664-302X. DOI: 10.3389/fmicb.2021.705310.

[51] Stephen T. Abedon and Rachel R. Culler. “Optimizing bacteriophage plaque fecundity”. In: *Journal of Theoretical Biology* 249.3 (Dec. 7, 2007), pp. 582–592. ISSN: 0022-5193. DOI: 10.1016/j.jtbi.2007.08.006. URL: https://www.sciencedirect.com/science/article/pii/S0022519307003815 (visited on 07/11/2025).

[52] J Yin. “Evolution of bacteriophage T7 in a growing plaque.” In: *Journal of Bacteriology* 175.5 (Mar. 1993), pp. 1272–1277. ISSN: 0021-9193. DOI: 10.1128/jb.175.5.1272-1277.1993. URL: https://www.ncbi.nlm.nih.gov/pmc/articles/PMC193211/ (visited on 07/11/2025).

[53] Mike S. Son and Ronald K. Taylor. “Growth and Maintenance of Escherichia coli Laboratory Strains”. In: *Current protocols* 1.1 (Jan. 2021), e20. ISSN: 2691-1299. DOI: 10.1002/cpz1.20. URL: https://www.ncbi.nlm.nih.gov/pmc/articles/PMC8006063/ (visited on 07/14/2025).

[54] J. J. Bull and I. J. Molineux. “Predicting evolution from genomics: experimental evolution of bacteriophage T7”. In: *Heredity* 100.5 (May 2008). Publisher: Nature Publishing Group, pp. 453–463. ISSN: 1365-2540. DOI: 10.1038/sj.hdy.6801087. URL: https://www.nature.com/articles/6801087 (visited on 07/14/2025).

[55] Jie Lin and Ariel Amir. “The Effects of Stochasticity at the Single-Cell Level and Cell Size Control on the Population Growth”. In: *Cell Systems* 5.4 (Oct. 25, 2017), 358–367.e4. ISSN: 2405-4712. DOI: 10.1016/j.cels.2017.08.015. URL: https://www.sciencedirect.com/science/article/pii/S2405471217303873 (visited on 04/23/2024).

[56] Holly Kloos Dressman and John W. Drake. “Lysis and Lysis Inhibition in Bacteriophage T4: rV Mutations Reside in the Holin t Gene”. In: *Journal of Bacteriology* 181.14 (July 1999), pp. 4391–4396. ISSN: 0021-9193. DOI: 10.1128/jb.181.14.4391-4396.1999. URL: https://www.ncbi.nlm.nih.gov/pmc/articles/PMC93942/ (visited on 07/11/2025).

[57] Benjamin Kerr et al. “Local migration promotes competitive restraint in a host–pathogen ’tragedy of the commons’”. In: *Nature* 442.7098 (July 2006). Publisher: Nature Publishing Group, pp. 75–78. ISSN: 1476-4687. DOI: 10.1038/nature04864. URL: https://www.nature.com/articles/nature04864 (visited on 07/09/2025).

[58] Pavitra Roychoudhury et al. “Fitness benefits of low infectivity in a spatially structured population of bacteriophages”. In: *Proceedings of the Royal Society B: Biological Sciences* 281.1774 (Jan. 7, 2014). Publisher: Royal Society, p. 20132563. DOI: 10.1098/rspb.2013.2563. URL: https://royalsocietypublishing.org/doi/10.1098/rspb.2013.2563 (visited on 07/09/2025).